

# Dynamics of Entangled Polymeric Fluids in Two-roll Mill studied via Dynamic Light Scattering and Two-color flow Birefringence. II. Transient flow

Subrata Sanyal<sup>†</sup>, Dmitry Yavich<sup>\*</sup> and L. Gary Leal

*Department of Chemical Engineering, University of California at Santa Barbara, Santa Barbara, CA 93106-5080, U.S.A.*  
(June 23, 2000)

We present an extensive experimental study of birefringence and velocity-gradient components for a series of high molecular weight, flexible, entangled polystyrene solutions subjected to transient start-up flows in a co-rotating two-mill to several Weissenberg numbers. The time-dependent changes in the polymer microstructure, as measured by a two-color flow birefringence technique, is shown to be very distinctly coupled with the transient response of the corresponding velocity-field, measured by a dynamic light scattering technique. As expected, polymer deformations induce substantial modifications from the Newtonian flow-field. As a result, measured values of both velocity-gradient components as well as flow-type parameter reduce, thereby drastically decreasing the extensional strength or measured Weissenberg number at the stagnation-point relative to the velocity-field for a Newtonian fluid. This result is very similar to that seen with dilute polymer solutions, although the mechanism responsible should be different. Both birefringence and flow-parameters show distinct undulations in their transient response which appear at earlier times with increased intensity as the Weissenberg number of the flow is increased. These undulations are shown to be strongly correlated to each other in time, indicating that the same underlying dynamics should be responsible for both. The transient variation of magnitude of the measured flow-parameters is found to be most pronounced for the polymer solution with the smallest number of entanglements per chain. Although the impact of the dynamics of both polymer on flow and flow on polymer are very complicated, their individual behaviors and the tight coupling between them are shown to be invariant to the changes in polymer concentration and molecular weight, provided that the number of entanglements per chain,  $N_e$  is held fixed. The dependence of the transient results on  $N_e$  is very similar to that found in the steady-state experiments on the same polymeric fluids (Sanyal, Yavich, and Leal, manuscript in preparation, 2000). The results presented in this paper are in close qualitative agreement with the recent theoretical predictions (Rummelgas and Leal, *J. Non-Newtonian Fluid Mech.* **90**, 187, 2000) using a reptation-based vector model.

## I. INTRODUCTION

Characterization of dynamics of entangled polymeric fluids subjected to macroscopic deformations imposed by a flow-field is of great importance for processing of polymers, with the objective of producing materials of desirable properties. In most cases, this requires to generate large deformation-induced anisotropy in the polymer microstructure, i.e., a strong alignment and stretch of the polymer chains along preferential directions. However, most experimental efforts on entangled polymers till date were restricted to cases that involve relatively small conformational changes, such as in viscometric flows, and there have been only a few studies of entangled polymers subjected to purely extensional and/or extension-dominated “mixed” flows [1] (also called “strong” flows, since the magnitude of the strain-rate exceeds the vorticity in these flows), where large deformations on the polymer conformation can be achieved. The primary reasons for this were, firstly, the difficulty in producing small-scale laboratory flows with such extensional characters, and secondly, the non-availability of simultaneous flow characterization procedures for such flows, compared to the case of nearly homogeneous viscometric flows where the flow-field does not change much from the simpler

Newtonian form and hence stress (or birefringence) can be measured and interpreted globally within the flow. An added reason for the lack of prior experiments with strong flows is that for complete characterization of dynamics one has to take into account of the tight coupling that exists between flow effects and polymer conformational effects. That is, when large deformations are imposed on a polymeric fluid, the same flow properties that cause the conformation of polymer molecules to change, are also affected by the changes of the polymer molecules. Thus, in order to produce meaningful data for the characterization of polymeric materials it is required to measure, simultaneously and independently, the polymer conformation as well as the properties of the flow-field.

On the theoretical frontier, most efforts in recent years were focused in developing molecularly based constitutive equations for entangled polymer solutions. In particular, the original Doi and Edwards (DE) reptation based tube model [2] was extended to include non-uniform chain-stretching to give rise to the so called Doi-Edwards-Marrucci-Grizzuti (DEMG) model [3,4]. Although very successful in predicting polymer dynamics for homogeneous flows, numerical simulations of these models for non-trivial flows become too complex and computationally non-tractable. In order to avoid this difficulty, many

simplified approximations [5,6] were suggested over the number of years, of which the latest one is that due to Remmelgas et al. [6], which proposed a single vector approximation to the DEMG model and separately treated the dynamics of stretch and orientation of the entangled polymers in flow, thereby making the numerical simulations of the same simpler.

The model comparison of experimental results on entangled polymeric solution subjected to steady-state or time-dependent flows in the past have followed the traditional rheological path of focusing on shear-flows [7,8], primarily because of the earlier-stated reason. On the other hand, for entangled polymeric fluids subjected to steady-state or time-dependent extension-dominated flows, the situation was far more complex, because even though the changes in the polymer conformation in such a flow could be measured with the use of a two-color flow birefringence (TCFB) technique [9], simultaneous unambiguous measurement of flow-parameters was not available until the advent of a dynamic light scattering (DLS) technique [9,10] in recent years. In absence of a full-fledged fluid mechanical calculation for the simultaneous prediction of flow-field and birefringence in such flows using the DEMG model, one useful way would be to compare the experimental birefringence results with that obtained from the numerical simulations of the DEMG model, by using the DLS measurements of the velocity-gradients as input to the model. This too have been possible only for steady-state flows [11,12] recently, and the work is underway to develop numerical codes for time-dependent flows [13]. In addition, the recent work of Remmelgas et al. [6] allows one to calculate prediction for the dynamics of both polymer microstructure and the flow simultaneously using a model which approximates the DEMG model, as noted earlier. In this respect, it is extremely important to create an experimental database for entangled polymers subjected to extension-dominated flows which will provide a unique basis to test the predictions from the aforementioned reptation based models.

With this in mind, the purpose of the present series of papers is to understand the dynamics of entangled, high molecular weight polymeric fluids subjected to the strong [1], extension-dominated flows generated at the stagnation-point of a co-rotating two-roll mill. An important characteristic of strong flows is that adjacent material points separate exponentially in time (and this is necessary to efficiently achieve high polymer extensions), rather than linearly as found in weak (shear) flows. We have undertaken an extensive study of a series of entangled polystyrene solutions, where the polymer conformation is measured with the use of a TCFB method [9] and the corresponding velocity-gradients of the flow-field are obtained by using a DLS technique [9,10] developed in our laboratory. The results from such a study are presented in the present series of papers. In the Part I [12] of this series, we have presented the results when the

polymeric fluids are subjected to steady-state flow conditions in a two-roll mill, where a detailed comparison of the TCFB results for the samples with the DEMG model [3,4] is also carried out. In this paper, we present transient measurements of the birefringence and velocity-gradient in start-up of a strong, extensional-type two-roll mill flow from rest, to gain useful insight about the time-evolution of the coupled dynamics of the polymer configuration and the imposed velocity-field from an initial condition to a steady-state.

The paper proceeds first by introducing in sec. II the experimental methods and the samples used in this study. The results from our time-dependent experiments are detailed in sec. III, where we begin (in sec. III.A) with characterizing the inception of flow with the use of a Newtonian fluid. We then show how the flow-field is modified relative to that expected for a Newtonian fluid by the presence of polymers. The measurements of the dynamical evolution of the birefringence, orientation angle, velocity-gradient and flow-type parameters following the start-up of a flow from rest for the three entangled samples of our study are described in sec. III.B. Section IV deals with the discussion of the results, where we compare the flow- and polymer-dynamics of the samples at similar rates of flow-deformations (i.e., Weissenberg numbers) in sec. IV.A, characteristic strains at the overshoot of birefringence for inception of flow in sec IV.B, and the measurements made at different positions in the gap between the rollers of the two-roll mill in sec IV.C. Finally, sec. V contains a summary of our findings and conclusion.

## II. EXPERIMENTAL METHODS AND MATERIALS

As described in Part I [12], we use three moderately entangled polystyrene solutions, PS81, PS82 and PS2, and a Newtonian fluid sample. The Newtonian sample is a suspension of polystyrene microspheres of diameter  $0.11\mu\text{m}$  in glycerol at a concentration of 150 ppm. As given in Table I, the entangled polymeric fluids are made by mixing high molecular weight fairly monodisperse ( $M_w/M_n \sim 1$ ) polystyrene samples in solvents. The solvents were prepared by adding polystyrene oligomer with  $M_w = 6000$  or  $2500$  and a broad molecular weight distribution to toluene at specific mixing ratios by weight (toluene: 2500 PS = 43:57 for PS81 and PS82, and 48:52 for PS2). The rheological measurements for simple shear flow were performed using the cone and plate geometry of Rheometrics RMS-800 rheometer with a cone diameter of 40 mm and a gap angle of  $4^\circ$ . The three polystyrene solutions along with their characteristic rheological parameters are listed in Table I, which is reproduced from Part I [12]. Here,  $M_w$  and  $M_n$  specify the weight-average and the number-average molecular weights respectively,  $c$  is the polystyrene concentration,  $\eta_0$  is the zero-shear

viscosity,  $N_e$  is the average number of entanglements per chain,  $\tau_R$  is the longest Rouse relaxation time, and  $n_t$  is the number of Kuhn statistical subunits in the chain calculated from the molecular weight of the polymer [14] based on the assumption of 10 monomers per subunit.

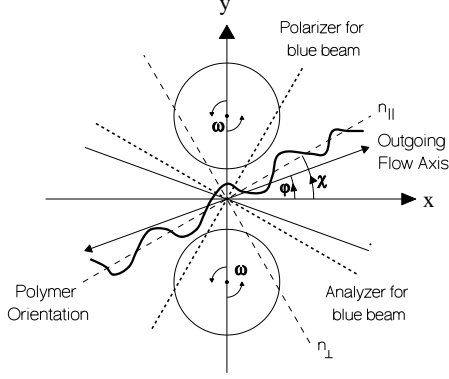


FIG. 1. Relative orientation of the optical system defined by the incident blue beam polarization, the flow-cell, and the definition of the flow-field coordinate system.

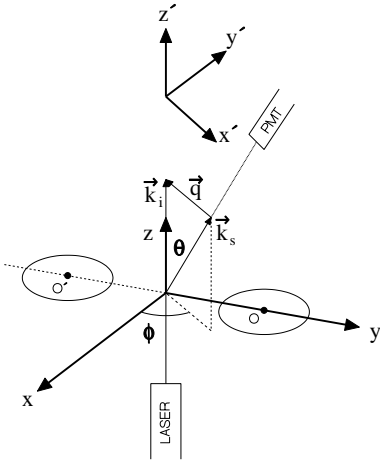


FIG. 2. Schematic representation of the dynamic light scattering configuration showing angle definitions, vector orientations, etc. The flow is in the  $xy$ -plane.

Our computer-controlled co-rotating two-roll mill is a flow device [15] where both rollers are driven simultaneously by a single stepping motor to generate strong

or extension-dominated flows in the region between the rollers. Fig. 1 shows the principal optical axes of the solution and the symmetry axes of the flow-field, as well as the relative orientation of the polarizer and analyzer for the blue laser beam (used in our flow birefringence experiments, as discussed below). Even though the flow is quite complex throughout the flow device, in our  $75\mu\text{m}$  diameter measuring region surrounding the stagnation-point in the central plane ( $xy$ -plane in Figs. 1 and 2) of the two-roll mill, the Newtonian velocity-field can be well approximated by a two-dimensional, linear (or homogeneous), symmetric form,

$$v = \nabla \vec{v} \cdot \vec{r} = \dot{\gamma} \begin{bmatrix} 0 & 1 \\ \lambda & 0 \end{bmatrix} \cdot \vec{r}, \quad (1)$$

in the coordinate system (Figs. 1 and 2) that is rotated through  $45^\circ$  relative to the principal axes of the rate of strain tensor. Here  $\dot{\gamma}$  is the magnitude of the velocity-gradient tensor (i.e.,  $\dot{\gamma} \equiv |\nabla \vec{v}|$ ) which is a linear function of the roller rotation rate for a Newtonian fluid at very low Reynolds numbers, and  $\lambda$  is the flow-type parameter which ranges from  $-1$  to  $1$ . Pure rotational flow corresponds to  $\lambda = -1$ , simple shear flow to  $\lambda = 0$  and pure extensional (or hyperbolic) flow to  $\lambda = 1$ . With the use of different pairs of rollers from a set of eight such pairs, which changes the ratio of the gap-width between the rollers to their radius, our two-roll mill is capable of producing mixed shear and extensional flows with  $0 < \lambda_N \leq 0.25$  for a Newtonian fluid, where the subscript “N” used for any parameter throughout this paper refer to the Newtonian-value of that parameter. The two-roll mill configuration used in all experiments reported in the present series of papers [12] correspond to  $\lambda_N = 0.1501$ , although as we will show below the actual flow-type changes with the use of polymer solutions due to strong flow-modification compared to the flow-field expected for a Newtonian fluid. In the stagnation region, the polymer has a large residual time and hence experiences large strain and strain-rates. These make it straightforward to highly stretch and align the polymer chains at the stagnation-point, and owing to the substantial residence time in the region of our measurement the polymer will reach a configuration consistent with the corresponding homogeneous flow. Thus, in the stagnation region, we expect to obtain a maximum degree of stretch of the polymer, and also a considerable degree of flow-modification from the Newtonian velocity-field.

As noted before, the two non-intrusive experimental methods used in this study are flow birefringence that provides a local measurement of the polymer configuration in the two-roll mill, and dynamic light scattering that measures the local velocity-gradients. The details of our entire experimental set-up comprising of these two optical techniques are described in Part I [12], and hence will not be repeated here.

In transient flow experiments both the degree of optical anisotropy (termed the birefringence,  $\Delta n$ ) and the orientation  $\chi$  of the principal axes of the refractive index tensor relative to axes  $[(x, y)$  in Figs. 1 and 2] fixed in the flow device are unknown and varying in time. The method of two-color flow birefringence [9], adopted in our laboratory, provides a means to simultaneously solve for  $\Delta n$  and  $\chi$  at each point in time in a single experiment. In this method, the two principal spectral lines of an argon-ion laser (green, with the wavelength of  $\lambda_G = 5145$  Å, and blue, with  $\lambda_B = 4880$  Å) are polarized  $45^\circ$  relative to each other and then passed in a collinear fashion along an identical optical path through the sample in a flow-cell which is placed between crossed polarizers for each beam. The extinction angle  $\chi$  is a measure of the average orientation of the Kuhn segments in the polymer fluids. A full description of the set-up and the data analysis procedure followed in the two-color flow birefringence experiments applied to two-roll mill flow device are previously detailed elsewhere [15].

The complete theory of the light scattering experiments relevant to our set-up can be found in Refs. [9,10]. Fig. 2 shows the orientation of the incoming light,  $\vec{k}_i$ , the scattered light,  $\vec{k}_s$ , and the scattering vector,  $\vec{q} = \vec{k}_i - \vec{k}_s$ . Provided that the seed particles are isotropic scatterers, and the time scale associated with the velocity-gradient [ $t_\gamma \sim (q\dot{\gamma}L)^{-1}$ , where  $L$  is the laser beamwidth] is much smaller than the time scale for diffusive motion [ $t_D \sim (Dq^2)^{-1}$ ], and the laser beam profile is Gaussian, the homodyne intensity auto-correlation function for a linear, two-dimensional flow of the form given by Eqn. (1) can be related to the velocity-gradient tensor. In particular, when the scattering vector  $\vec{q}$  is oriented parallel to the  $x$  axis, i.e.,  $\phi = 0^\circ$  [see Fig. 2], the homodyne intensity auto-correlation function reduces to

$$F_2(\vec{q}, t) = \beta \exp \left\{ -\frac{1}{2} q^2 \dot{\gamma}^2 L^2 t^2 \cos^2 \left( \frac{\theta}{2} \right) \right\}, \quad (2)$$

and when  $\vec{q}$  is oriented along  $y$  axis, i.e.,  $\phi = 90^\circ$ , then

$$F_2(\vec{q}, t) = \beta \exp \left\{ -\frac{1}{2} q^2 \dot{\gamma}^2 \lambda^2 L^2 t^2 \cos^2 \left( \frac{\theta}{2} \right) \right\}, \quad (3)$$

where  $\beta$  is a coherence factor for isotropic scatterers, and the scattering angle  $\theta$  and the flow-cell orientation angle  $\phi$  define the scattered beam relative to the coordinates of the flow-cell, as shown in Fig. 2. Thus, it is clear from Eqns. (2) and (3) that  $\dot{\gamma}$  and  $\lambda$  can be obtained from the exponential decay rates of the intensity auto-correlation functions independently measured at these two special orientations of the two-roll mill.

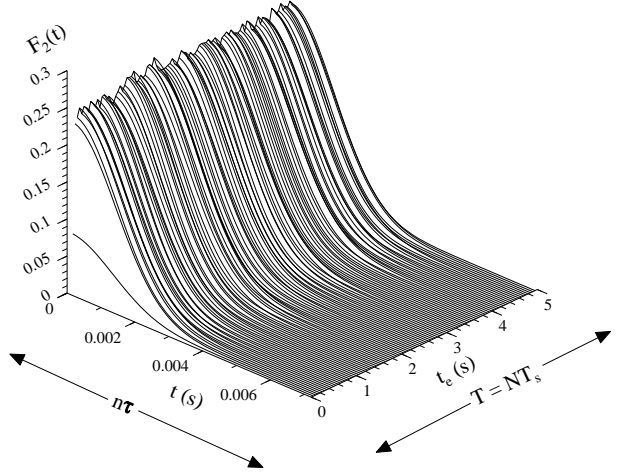


FIG. 3. Typical time-resolved intensity auto-correlation functions for the Newtonian fluid in the startup of a steady flow, measured at the stagnation-point of a two-roll mill with  $\lambda_N = 0.1501$ , apparent scattering angle  $\theta' = 22^\circ$ , roller orientation  $\phi = 0^\circ$ , angular velocity of the rollers  $\omega = 1.885$  rad/s. The correlator sample duration and the delay time are  $T_s = 0.05$  s and  $\tau = 100\mu\text{s}$ , respectively.

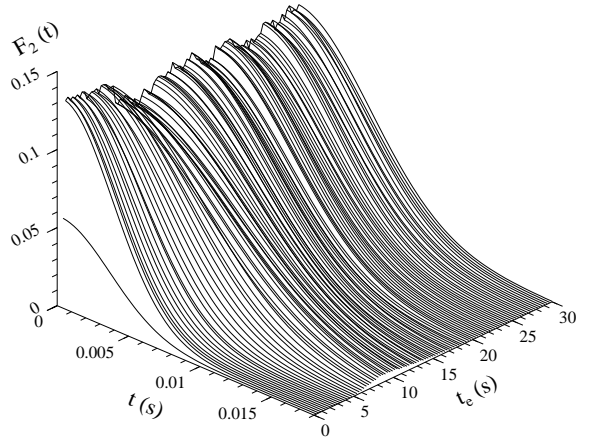


FIG. 4. Typical time-resolved intensity auto-correlation functions for the polystyrene solution PS82 in the startup of a steady flow with  $\lambda_N = 0.1501$  at the angular velocity of the rollers  $\omega = 0.2513$  rad/s (or the measured Weissenberg number,  $Wi_R = \dot{\gamma}\lambda^{1/2}\tau_R = 0.384$ ). In every  $T_s = 0.3$  s, one correlation function is registered at  $\phi = 0^\circ$ ,  $\theta' = 19^\circ$ . The correlation delay time is  $\tau = 250\mu\text{s}$ .

For the transient flow experiments, we use the data analysis technique described in Ref. [10]. Here, we men-

tion a few salient features related to these time-resolved experiments. First, the correlation delay time  $\tau$  should be so chosen that each correlation function decays completely over the  $n = 72$  channels of the correlator, i.e.,  $F_2(t = n\tau)/F_2(t = 0) \sim 10^{-3}$ . The predetermined total transient evolution time,  $T$ , of the flow to be studied is divided into  $N$  parts, and then  $N$  correlation functions are collected in this period of time, each for an evolution time of  $T_s = T/N$  (Fig. 3). The sampling time,  $T_s$ , over which each correlation function is collected must exceed the decay time,  $n\tau$ , of the correlation function, for the correlation function to be valid. The exponential decay rate of each such valid correlation function can then provide the velocity-gradient component at that particular instant of the evolution time,  $t_e$ . Second, it is desirable that the flow should not change substantially over the sampling time-period,  $T_s$ , so that the correlation function can be well approximated by a single exponential as in Eqns. (2) or (3), depending on the orientation of the two-roll mill. This resolution of time can be obtained via the choice of  $N$ . Third, each experiment over the total evolution time,  $T$ , consisting of  $N$  correlation functions (or  $N$  values of velocity-gradient components) should be repeated several times (typically, 200 times at high motor speeds to about 800 times at low motor speeds for the polymer samples) to form a statistically reasonable correlation function for each sampling time interval,  $T_s$ . The rest time of the motor in between two such consecutive repetition should be long enough so that the polymers can relax to the equilibrium state as in the beginning of the first experiment of the set. Finally, it is always advisable to compare the long-time limit (i.e., in the limit of evolution time  $t_e \rightarrow T$ ) of the transient flow-parameters with independently performed steady-state measurements, where the data are collected and averaged after the motor has run for a time-period very much longer than  $T$ , to check if the transient flow has actually reached the corresponding steady-state in the total predetermined evolution time,  $T$ .

To exemplify these features, we present the typical three-dimensional plots of the time-resolved correlation functions obtained for the start-up flow for a Newtonian fluid (Fig. 3), as well as for a polymeric fluid, PS82 (Fig. 4), in the two-roll mill. The angular roller velocity and the apparent scattering angles were  $\omega = 1.885$  rad/s,  $\theta' = 22^\circ$  and  $\omega = 0.2513$  rad/s,  $\theta' = 19^\circ$ , respectively for the Newtonian sample and PS82. The apparent scattering angle  $\theta'$  is different from  $\theta$  owing to the refraction by the sample in the flow-cell. A more detailed discussion of the results obtained from these figures will be done in the next section. At this point it is sufficient to note that these two three-dimensional plots clearly indicates the distinctly different dynamical evolution of the flow-field for the Newtonian and the polymeric fluid, as expected, on the inception of flow. As shown in Fig. 4, in order to obtain valid (exponential) time-resolved correlation func-

tions, for polymeric fluids used in our experiments, that satisfy all the criteria mentioned above, we had chosen the total evolution time,  $T \sim 30$  s (in similarity with the total evolution time for the corresponding transient birefringence experiments [11], as well as that used before for other polymeric fluids in our laboratory [15–17]), the sampling time,  $T_s \sim 0.3$  s (and hence  $N \sim 100$ ), the correlation delay time,  $\tau = 250\mu\text{s}$ , and about 3 mins of rest time of the motor between two consecutive transient runs. Thus, the total experimental time, inclusive of the repetitions for statistical averaging, varied from about 10 hrs. for experiments with low motor speeds to about 50 hrs. for that with high motor speeds. It was shown in Part I [12] that the long-time value of the flow-parameters in our  $T = 30$  s transient experiments are within 10% – 15% of their value obtained from the corresponding steady-state experiments performed independently at the same motor speed, where the data collection started only after the motor has run for  $\geq 2$  mins. The results in Fig. 3 and 4 are obtained by averaging over a set of 200 and 500 repetitions, respectively.

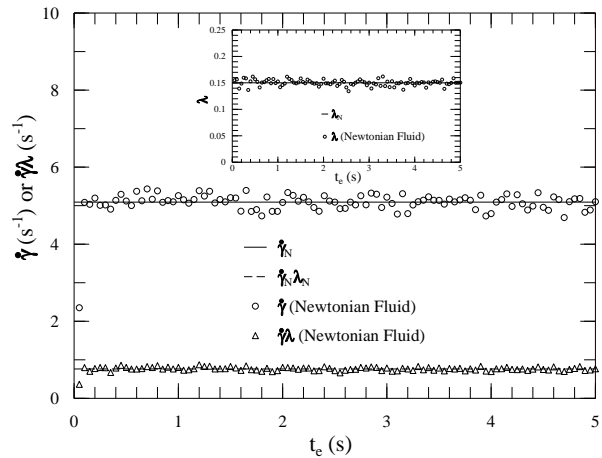


FIG. 5. The magnitude of the time-dependent velocity-gradients  $\dot{\gamma}$  and  $\dot{\gamma}\lambda$  deduced from the correlation functions at  $\phi = 0^\circ$  (the correlation delay time  $\tau = 100\mu\text{s}$ ), and  $\phi = 90^\circ$  ( $\tau = 400\mu\text{s}$ ), respectively in startup of a steady flow for the Newtonian sample corresponding the case shown in Fig. 2. The inset shows the time-dependence of the corresponding flow-type parameter  $\lambda$  obtained by point to point division of  $\dot{\gamma}\lambda$  by  $\dot{\gamma}$ . The straight lines represent the creeping flow solutions.

For the experiments with the Newtonian fluid in Fig. 3, the choice of the correlation delay time  $\tau = 100\mu\text{s}$  was made similarly to the case of polymeric fluids, i.e., by checking the correlation functions in the preliminary experiments to decay by 3 to 4 orders of magnitudes over

the fixed decay time of  $72\tau < T_s$  of our correlator at all evolution time,  $t_e$ . This sets a lower limit on  $T_s$  which our choice of  $T_s = 0.05$  s does satisfy. The choice of  $N = 100$  was made in similarity with Fig. 4 and hence the total evolution time in this case is  $T = NT_s = 5$  s.

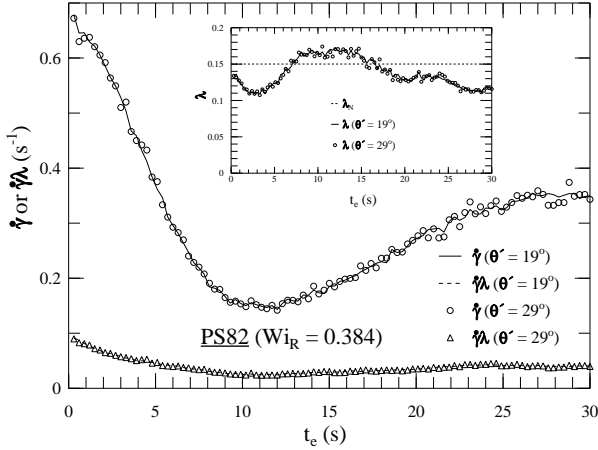


FIG. 6. The magnitude of the time-dependent velocity-gradients  $\dot{\gamma}$  and  $\dot{\gamma}\lambda$  extracted from the correlation functions at  $\phi = 0^\circ$  (the correlation delay time  $\tau = 250\mu\text{s}$ ) and  $\phi = 90^\circ$  ( $\tau = 1000\mu\text{s}$ ), respectively in startup of a steady flow for the polystyrene sample PS82 corresponding to the case shown in Fig. 3. Two sets of data, with the symbols explained in the figure, represent the results from two identical set of experiments at the apparent scattering angles of  $\theta' = 19^\circ$  and  $\theta' = 29^\circ$ . The inset shows the time-dependence of the corresponding flow-type parameter  $\lambda$ , obtained by point to point division of  $\dot{\gamma}\lambda$  by  $\dot{\gamma}$ , compared to the constant  $\lambda_N = 0.1501$ .

### III. RESULTS

For a concentrated polymer solution, as we have mentioned before, because of the complicated interaction between the changes in the polymer configuration and its impact on the flow-field and vice versa, it is very crucial that both polymer conformation and flow kinematics be measured. In this section, we will present experimental birefringence and dynamic light scattering results obtained for the entangled polymeric solutions subjected to time-dependent flows, in particular, to start-up flows from rest for the two-roll mill configuration which corresponds to a Newtonian flow-type parameter,  $\lambda_N = 0.1501$ . The two-color flow birefringence results, namely, birefringence,  $\Delta n$ , and orientation angle,  $\chi$ , versus evolution time,  $t_e$ , will provide information about the dynamical evolution of the polymer conformation following the onset of flow from rest. On the other hand, the flow-parameters, namely, the velocity-gradient,  $\dot{\gamma}$ , and the

flow-type parameter,  $\lambda$ , plotted against evolution time, obtained from DLS experiments, will depict corresponding changes in the flow kinematics. In Part I [12], the flow was shown to approximately retain its symmetry, even for our polymer experiments, in the range of dimensionless rates of flow-deformation (i.e., Weissenberg numbers) studied here. Thus, our DLS data analysis procedure [10], which is rigorously valid for seeded Newtonian fluids, can be applied for the transient flow experiments with polymeric fluids, presented here.

#### A. Flow characterization and flow-modification

Our implementation of the two-color flow birefringence technique was primarily developed to study the response of polymeric fluid samples subjected to time-dependent flows, because of its capability of fast, point-wise measurements of the optical anisotropy of the fluid, with a very good reproducibility. The dynamic light scattering technique, on the other hand, provides the capability of real-time, point-wise measurements of the time-dependent response of the flow-parameters to an imposed flow-field. Before proceeding with the experiments on polystyrene solutions, it is crucial that the Newtonian flow-field at the stagnation-point (where the birefringence experiments are generally conducted) is known, so that one can quantify the changes in the measured flow-fields due to non-Newtonian behavior of the polymers. It is necessary that the two-roll mill be capable of creating well-defined flow-field with a Newtonian fluid. For the transient start-up flow with a Newtonian fluid, this would mean that the flow should instantaneously attain its steady-state value, which can be calculated using the theoretical creeping flow solution [16] (as discussed in Part I). The creeping flow solutions for the flow-parameters are direct functions of the geometry of the two-roll mill. In all our time-dependent flow experiments reported in this paper, the maximum acceleration possible with our motors (100,000 steps/s) was used to ramp it up from rest. The typical picture of the evolution of the time-resolved correlation functions at the onset of flow in our flow characterization experiments with the Newtonian fluid is shown in Fig. 3. The detailed nature of the time-resolved correlation functions for both parallel ( $\phi = 0^\circ$ ) and perpendicular ( $\phi = 90^\circ$ ) orientations of the two-roll mill are quite similar and hence we showed only one of them,  $\phi = 0^\circ$ , here. The velocity-gradient components,  $\dot{\gamma}$  and  $\dot{\gamma}\lambda$ , at each instant of evolution time,  $t_e$ , is extracted from the decay rates of the fitted exponential functions of Eqn. (2) and (3) to these measured correlation functions. The value of the laser beamwidth,  $L$ , used here is obtained from a calibration procedure that is described in Part I. In order to verify that the experimentally obtained correlation functions are very close to exponential in nature so that the above

procedure is indeed justified, we required a correlation coefficient  $R^2$  specifying the quality of fit exceeding 0.99. The extracted velocity-gradient components from Fig. 3 are shown in Fig. 5. We see that except for the first point at  $T_s = 0.05$  s, both  $\dot{\gamma}$  and  $\dot{\gamma}\lambda$  have reached their steady-state value, which is maintained throughout the experiment. In fact, from the second point onwards, all data for these two parameters lie within 11% of the theoretical creeping flow solutions [12,16],  $\dot{\gamma}_N$  and  $\dot{\gamma}_N\lambda_N$ , shown by the straight lines. Also, it is clearly shown in the inset that the time-evolution of the flow-type,  $\lambda$ , obtained by dividing  $\dot{\gamma}\lambda$  by  $\dot{\gamma}$  at each evolution time, is very close to its theoretical value  $\lambda_N = 0.1501$ . The initial delay in the onset of flow, as noted in the earlier work [10], is due to the finite time-scale for vorticity diffusion in the Newtonian fluid. Thus, we have clearly shown that the two-roll mill is capable of creating a constant well-characterized flow-field in the stagnation-point. Further, the start-up is almost instantaneous and limited solely by the ramp-up acceleration of the motor and the time-scale associated with diffusion of vorticity in the fluid.

To see how  $\dot{\gamma}$ ,  $\dot{\gamma}\lambda$  and  $\lambda$  evolve with time in the case of a non-Newtonian viscoelastic sample, let us consider the representative case of the sample PS82 subjected to the start-up of a flow shown in Fig. 4, and extract the flow-parameters in an exactly similar fashion as discussed above. Fig. 6 presents the result, deduced from Fig. 4, where as shown by the solid and broken lines respectively, following the start-up, both  $\dot{\gamma}$  and  $\dot{\gamma}\lambda$  decrease in time to reach a minimum and then again increase to reach their approximate steady-state value (which is lower than the initial value) at a longer evolution time. The inset shows the time-dependence of  $\lambda$  as obtained by dividing  $\dot{\gamma}\lambda$  by  $\dot{\gamma}$ , point by point. Owing to a much higher viscosity of polystyrene samples compared to the Newtonian fluid, the vorticity diffusion time-scale in this case is comparatively much smaller and hence the initial value of  $\dot{\gamma}$  is very close to the Newtonian-value. The initial value of the second correlation function in Fig. 4 is different from the rest, reflecting a different value of the coherence factor,  $\beta$ , although its decay rate similar, thus yielding a similar value of  $\dot{\gamma}$ . The presence of polymer is clearly making an impact upon the flow-type parameter (and hence on  $\dot{\gamma}\lambda$ ) from the very beginning of the flow-evolution. The parameter  $\lambda$  follows a complex time-evolution and shows an oscillation around the corresponding Newtonian-value of  $\lambda_N = 0.1501$ . Its value is lower than  $\lambda_N$  almost always, except when both  $\dot{\gamma}$  and  $\dot{\gamma}\lambda$  show minimum between  $t_e = 7$  s and  $t_e = 15$  s. These curves, when compared to the corresponding ones for the Newtonian fluid (Fig. 5), provide a clear indication that the entangled polystyrene samples very significantly modify the otherwise Newtonian flow. In Fig. 6, we have also provided results obtained by repeating the same experiment when the apparent scattering angle  $\theta'$  is changed from  $19^\circ$  to  $29^\circ$ . The time-profile for each flow-parameter is very

well reproduced within an experimental error limit of 9%. This provides a direct proof of the fact that the transient flow conditions with these entangled samples are quite repeatable and the data obtained in the light scattering experiments for such flows are well reproducible inside the range of apparent scattering angle ( $19^\circ \leq \theta' \leq 29^\circ$ ) used in the present study.

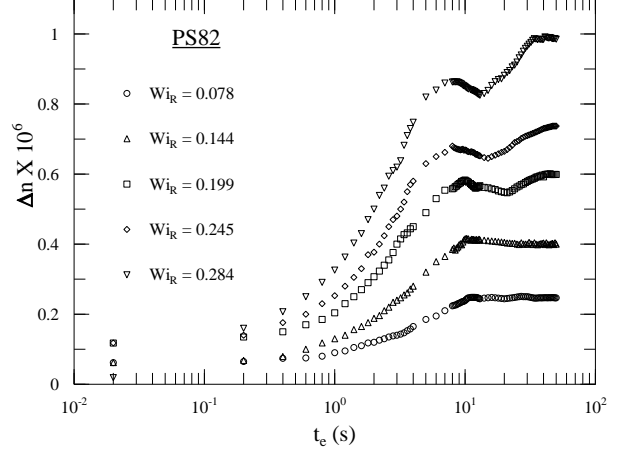


FIG. 7. Time-dependent birefringence on inception of a two-roll mill flow ( $\lambda_N = 0.1501$ ) for PS82 at several Weissenberg numbers,  $Wi_R = \dot{\gamma}\lambda^{1/2}\tau_R$ , based on the measured steady-state values of  $\dot{\gamma}$  and  $\lambda$ , and the Rouse time,  $\tau_R$ .

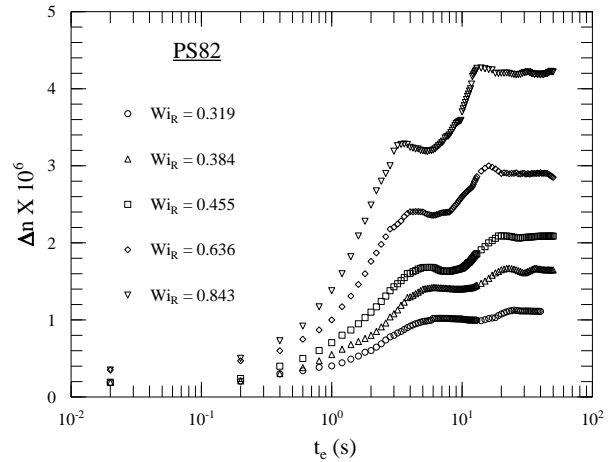


FIG. 8. Same as Fig. 7, but at higher Weissenberg numbers,  $Wi_R = \dot{\gamma}\lambda^{1/2}\tau_R$ .

In prior work from this laboratory [8,11], the non-

dimensionalized measure used to identify transient flow experiments was the Weissenberg number of the flow,  $(Wi_R)_N = \dot{\gamma}_N \sqrt{\lambda_N} \tau_R$ , based on the Newtonian-values of the velocity-gradient,  $\dot{\gamma}_N$ , and the flow-type parameter,  $\lambda_N$ . This was done because of the unambiguous relationship between  $\dot{\gamma}_N$  and the roller speed  $\omega$  given by the creeping flow solution [16]. In reality, however, the Weissenberg number,  $Wi_R = \dot{\gamma} \sqrt{\lambda} \tau_R$ , based on the measured values of  $\dot{\gamma}$  and  $\lambda$ , is expected to be different for different polymeric fluids even if the imposed roller speed is the same. The velocity-gradient parameters measured in the independently performed steady-state experiments (as discussed before) are used to calculate the actual Weissenberg number,  $Wi_R$ , which are in turn used to identify our transient experiments. Table II lists the Newtonian and the measured values of the Weissenberg numbers used in our study for three polystyrene samples. The decreased value of the measured  $Wi_R$  compared to its Newtonian-value,  $(Wi_R)_N$ , is obviously a direct consequence of the flow-modification. The percentage difference of  $Wi_R$  relative to  $(Wi_R)_N$ , also given in Table II, shows that the flow-modification is very substantial in all the cases studied. There is a decreasing trend with the increase in the rate of deformation for the two polystyrene fluids with the similar number of entanglements, PS81 and PS2, and an increasing trend with PS82. We note that the range of Weissenberg numbers chosen for each of the three polystyrene samples are very different when compared to each other. This is so because, firstly, the choice of roller speeds (in rad/s) achievable in our two-roll mill set-up is restricted with the choice of motor (i.e., the motor speeds available in steps/s) and the worm-gear assembly attached between the motor and the two-roll mill. Secondly, based on our preliminary calculations of the number of entanglements per chain,  $N_e$ , for three samples, we did not expect the longest Rouse relaxation time,  $\tau_R$ , would be so different for the sample PS2 (see, Table I) compared to the other two. The linear viscoelastic experiments [12] to extract  $\tau_R$  of these fluids were performed only after the TCFB experiments. Finally, the flow-modification was much stronger than we expected. This, as can be seen from Table II, has further reduced the values of the measured Weissenberg numbers. Thus, even though our initial motor speeds (in steps/s) were very similar for all samples, the final measured Weissenberg numbers are very different. We also note that the strain-rate  $\dot{\gamma} \sqrt{\lambda}$  (used in calculating  $Wi_R = \dot{\gamma} \sqrt{\lambda} \tau_R$ ) provides a measure of the rate of stretch of material points along the direction of the outflow axis of the flow of Eqn. (1) [see, Fig. 1] from the stagnation-point. This means that the  $Wi_R$  used here or the  $(Wi_R)_N$  used in earlier reports [8,11], provides the steady-state value of the deformation rate which can be achieved in transient experiments only in the long-time limit, when the polymer chain is finally oriented along the principal eigenvector direction. At earlier times, when

the flow is evolving with time, the appropriate measure of the non-dimensionalized rate of deformation should be the *transient* Weissenberg number,  $Wi_R^{tr} = \dot{\gamma}(1 + \lambda)\tau_R$ , based on the transient strain-rate  $\dot{\gamma}(1 + \lambda)$ , instead of its steady-state value,  $\dot{\gamma} \sqrt{\lambda}$ .

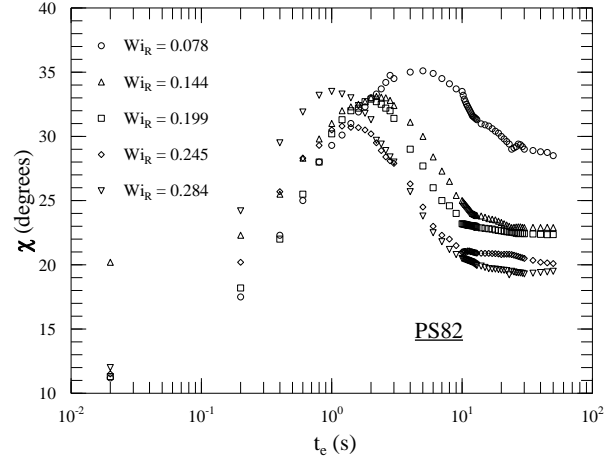


FIG. 9. Flow-induced extinction angle,  $\chi$  versus evolution time  $t_e$  for PS82 at different values of measured Weissenberg numbers.

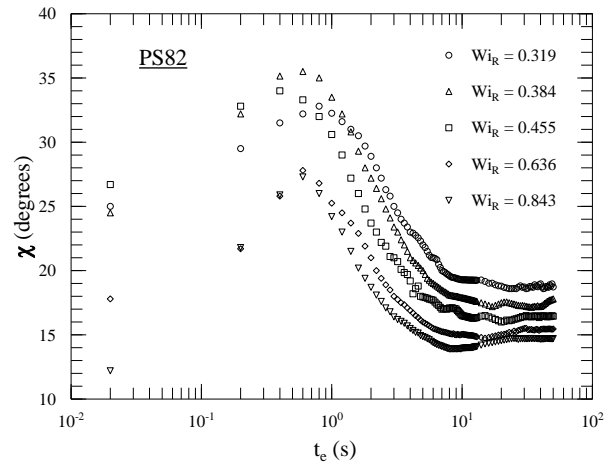


FIG. 10. Same as Fig. 9, but at higher measured Weissenberg numbers,  $Wi_R = \dot{\gamma} \lambda^{1/2} \tau_R$ .



## B. Dynamic evolution of birefringence and flow

As noted earlier, both the birefringence and the components of the velocity-gradients were measured in a region surrounding the stagnation-point of the flow-cell midway between the two rollers, where polymer chains can highly stretch and align. Also, because of the substantial residence time in this region, the polymer will reach a configuration consistent with the corresponding homogeneous flow. The complicated dynamics of the evolution of polymer configuration and flow-field, and their tight coupling require that we show simultaneously the measured birefringence, orientation angle and the corresponding flow-parameters plotted against evolution time,  $t_e$ , for the three entangled polystyrene fluids, at several different Weissenberg numbers.

We will first look into the features of the birefringence and flow data in general terms for each polystyrene fluids. A more detailed discussion and a comparison of results amongst the samples will be done in a later section. Let us first consider the case of PS82, the solution with about 7 entanglements per chain (see, Table I). Figs. 7 and 8 show the temporal-evolution of birefringence on inception of flow to a total of ten measured Weissenberg numbers spanning a range from 0.078 to 0.843 [ $0.099 \leq (Wi_R)_N \leq 1.782$ ]. The intrinsic difficulty associated with our transient birefringence experiment, namely, the appearance of multiple orders in the retardance, makes interpretation of results at high deformation rates extremely difficult and thus limits the highest value of the Weissenberg number for which the experiment could be performed. At the smallest  $Wi_R$ , the birefringence increases almost monotonically until a steady-value is reached. At higher values of  $Wi_R$ , the temporal-evolution of birefringence displays a series of undulations. Before reaching the long-time value, the birefringence trace goes through a notch at  $Wi_R = 0.144$ . At higher  $Wi_R$ , this notch gives rise to a very distinct peak (or overshoot), which progressively appears at earlier times with increased magnitude and intensity as  $Wi_R$  is increased. We note that the peak-time,  $t_p$ , of the first overshoot of birefringence in PS82 have reduced from  $t_p \approx 10$  s at  $Wi_R = 0.199$  to  $t_p \approx 3.55$  s at  $Wi_R = 0.843$ . Also, the long-time value of the birefringence monotonically increases with the increase in the rates of flow-deformation. These typical features are in agreement the observations in earlier studies with concentrated polymeric fluids for the inception of both shear flows [7,8] and extension-dominated flows [18] at large enough rates of deformation. At still higher  $Wi_R$ , this overshoot is followed by a very distinct trough (or undershoot) and then a second overshoot, each of which appear at an earlier time and become more distinct with increasing  $Wi_R$ . These features too are consistent with the prior observation by Geffroy *et al.* [18], but compared to their results

the dynamical evolution of the birefringence in this case has quite a few dissimilarities: the magnitude of the second overshoot and the long-time value of birefringence here is significantly higher than the magnitude of the first overshoot.

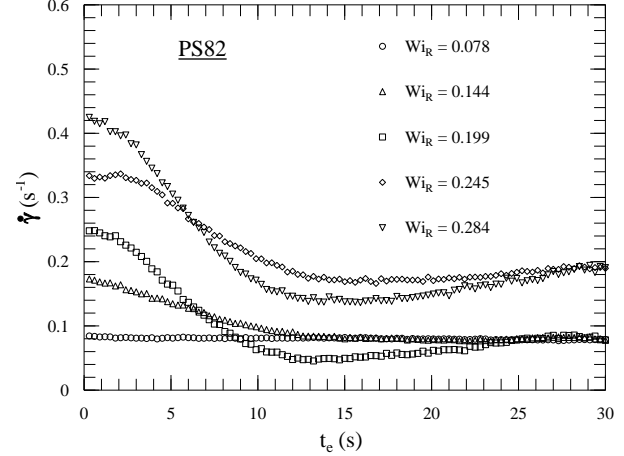


FIG. 11. Plot of the velocity-gradient component,  $\dot{\gamma}$  (deduced from the correlation functions at the two-roll mill orientation of  $\phi = 0^\circ$ ), as a function of evolution time,  $t_e$ , for start-up experiments with the sample PS82 at different measured steady-state  $Wi_R$ .

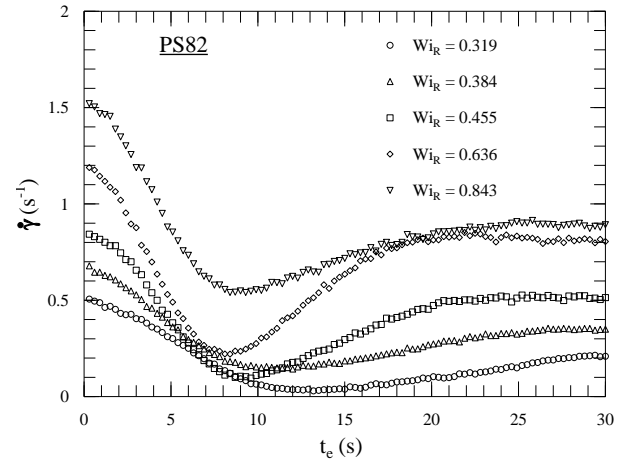


FIG. 12. Same as Fig. 11, but at higher measured Weissenberg numbers,  $Wi_R = \dot{\gamma} \lambda^{1/2} \tau_R$ .

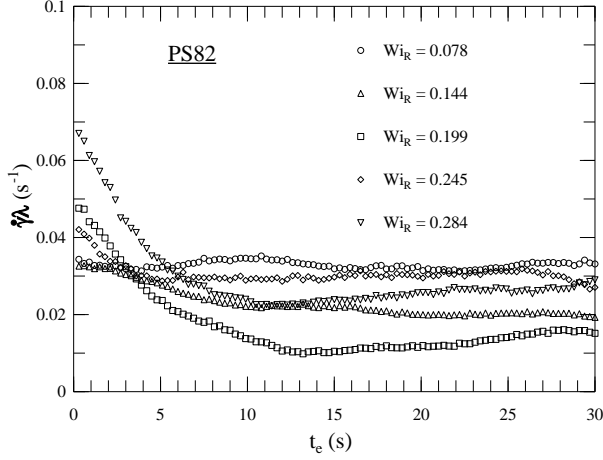


FIG. 13. Time-dependent velocity-gradient component,  $\dot{\gamma}\lambda$ , for PS82, extracted from correlation functions in start-up of steady flows at the two-roll mill orientation of  $\phi = 90^\circ$ , and at different measured Weissenberg numbers.

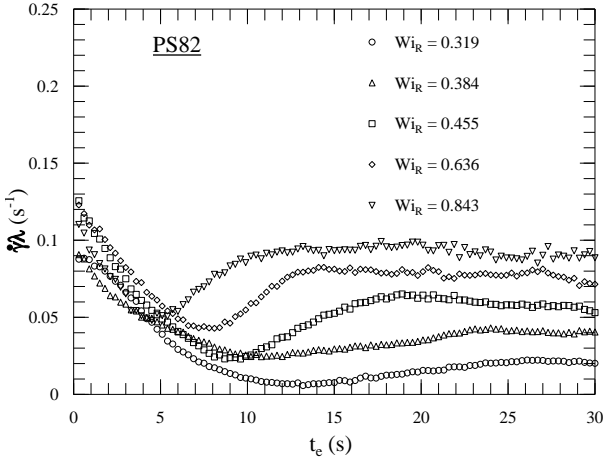


FIG. 14. Same as Fig. 13, but at higher values of the measured Weissenberg numbers.

The corresponding orientation angle data are shown in Figs. 9 and 10. For all cases, we should expect that the orientation angle,  $\chi$ , should initially have a value of  $45^\circ$ , i.e., it should coincide with the principal axis of the rate of strain tensor [Fig. 1]. In our experiments, the orientation angle at the onset of the flow is dominated by the residual anisotropy of the glass in the flow-cell window. The orientation angle reaches a maximum value in time as the anisotropic contribution of the polymer becomes

dominant. Keeping with the earlier studies for start-up of both shear [7,8] and extension-dominated flows [18], at low Weissenberg numbers, the orientation angle almost monotonically decreases to its long-time value, but at high enough  $Wi_R$ , it shows an undershoot just after the first overshoot in birefringence takes place. At large values of  $Wi_R$ , we may expect that the polymer molecules will become oriented close to the outflow axis of the flow-field. For a Newtonian fluid, the corresponding asymptotic value of  $\chi$  is  $\chi(Wi_R \rightarrow \infty) = \chi_\infty = \tan^{-1}(\sqrt{\lambda_N}) = 21.2^\circ$ . For the polymeric fluids, we may still try to find the values of  $\chi_\infty$  with the use of the above relation with  $\lambda_N$  replaced by the asymptotic value,  $\lambda_\infty$ , of the measured flow-type parameter, so that the flow-modification is taken into account. This could be done since, as shown in Part I, the flow approximately retains its symmetry in our experiments with entangled fluids. As expected,  $\chi_\infty$  in Figs. 9 and 10 decreases faster with the increase in Weissenberg number at smaller Weissenberg numbers, but this decrease almost saturate at higher Weissenberg numbers. At the highest  $Wi_R$ ,  $\chi_\infty \sim 14.8^\circ$ . The orientation angle curves at intermediate values of  $Wi_R$  also show some undulations before reaching the final asymptotic values, which are well-correlated in time to the first undershoot and the second overshoot in the corresponding birefringence traces.

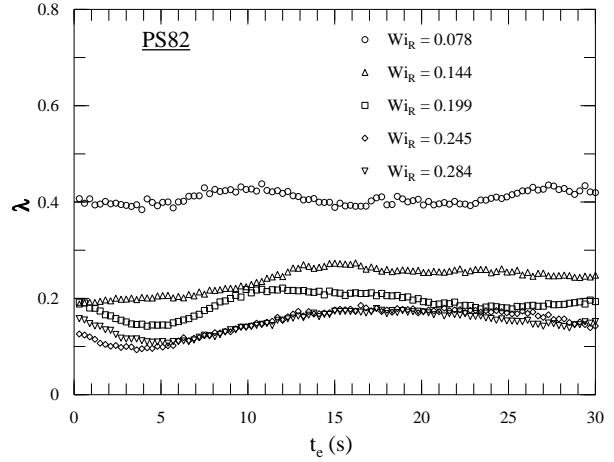


FIG. 15. Inception of the flow-type parameter,  $\lambda$ , for PS82, deduced from the ratio of the square root of the exponential decay rates of two corresponding correlation functions at different Weissenberg numbers,  $Wi_R = \dot{\gamma}\lambda^{1/2}\tau_R$  (based on the measured steady-state values of  $\dot{\gamma}$  and  $\lambda$ ).

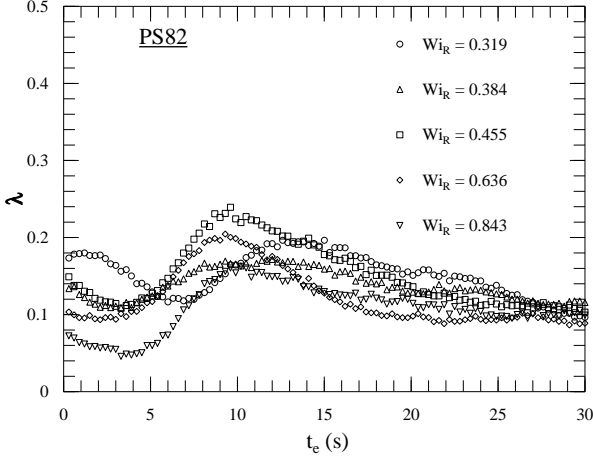


FIG. 16. Same as Fig. 15, but at higher values of the measured Weissenberg numbers.

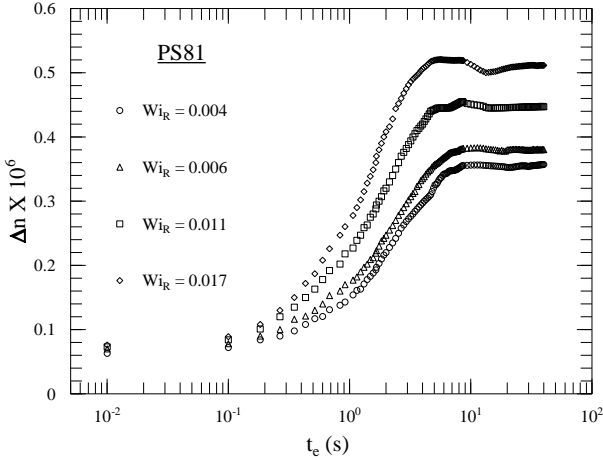


FIG. 17. Inception of birefringence as a function of evolution time,  $t_e$ , for sample PS81 at different measured steady-state Weissenberg numbers,  $Wi_R = \dot{\gamma}\lambda^{1/2}\tau_R$ .

In Figs. 11, 12 and Figs. 13, 14, respectively, we show the measured  $\dot{\gamma}$  and  $\dot{\gamma}\lambda$  versus the evolution time  $t_e$  for PS82 at the Weissenberg numbers for which we have shown the birefringence results above. From these figures, we extract the dynamical evolution curves for the flow-type parameter,  $\lambda$ , as shown in Figs. 15 and 16. At the lowest  $Wi_R$ ,  $\dot{\gamma}$  does not show any appreciable change from its Newtonian-value over the entire evolution time, but with the increase of  $Wi_R$ , there is a strong deviation in time from the Newtonian flow. The curves for

$\dot{\gamma}$  “start” from the Newtonian-value (which are higher at higher  $Wi_R$ , as expected), pass through a minimum (or undershoot) and then again increase to the respective long-time values, which are lower than the initial Newtonian-values at the same  $Wi_R$ . The minimum of the undershoot oscillates around  $t_e \sim 14$  s for  $Wi_R \leq 0.319$ , but beyond that, it progressively appears at earlier time until  $Wi_R = 0.636$ . At this deformation rate and above, the minimum of the undershoot in  $\dot{\gamma}$  appears at  $t_e \sim 8$  s. The strength of the undershoot, as well as the asymptotic value of  $\dot{\gamma}$  increases with the Weissenberg number. At the two lowest  $Wi_R$ ,  $\dot{\gamma}\lambda$  (Fig. 13 and 14) and hence  $\lambda$  (Fig. 15 and 16) show very little variation in their values following the onset of the flow, but surprisingly, these values are higher than that expected with a Newtonian fluid. As we will show and discuss about it in the following, this behavior takes place repeatably at low Weissenberg number flows for all three entangled solutions studied. For the velocity-gradient component,  $\dot{\gamma}\lambda$ , too the intensity of the undershoot increases with increasing rate of deformation and also it progressively appears at earlier times. We have noted that the initial magnitude of the velocity-gradient component  $\dot{\gamma}$  is always very close but slightly less than the Newtonian value,  $\dot{\gamma}_N$ . In contrast, the initial value of  $\dot{\gamma}\lambda$  for higher rates of deformation is such that the initial value for  $\lambda$  oscillates around the  $\lambda_N$  and then reduces substantially from the same at the highest Weissenberg numbers. At low rates of flow-deformation, the flow-type parameter shows an undershoot at  $t_e \sim 5$  s before reaching the long-time value by  $t_e \sim 15$  s, but at high rates, apart from the presence of this undershoot, an overshoot shows up at  $t_e \sim 10$  s before the flow-type parameter reaches the asymptotic limit by  $t_e \sim 25$  s. There is a transition between these two types of behaviors at  $Wi_R = 0.319$ , where the extremum of both the undershoot and the following overshoot are shifted to the later times. The asymptotic value,  $\lambda_\infty$ , of the flow-type parameter also shows a difference in behavior below and above this  $Wi_R$ . In particular,  $\lambda_\infty$  decreases as  $Wi_R$  is increased till  $Wi_R = 0.319$ , but for higher values of  $Wi_R$ , it remains almost constant,  $\lambda_\infty \sim 0.1$ .

In Figs. 17, 18 and Figs. 19, 20, we show the temporal-evolution of the birefringence and orientation angle, respectively, for the start-up of the two-roll mill flow to several different Weissenberg numbers with the polystyrene fluid PS81, which has approximately 13 entanglements per chain. At low Weissenberg numbers, similar to the results shown above for sample PS82, both birefringence and orientation angle (after overcoming the residual glass anisotropy) show smooth transitions towards their long-time values. On the other hand, at high rates of deformation, the time-dependent configurational dynamics for PS81 is very much different compared to that of PS82, as apparent from these figures. The overshoot and the following undershoot in the birefringence curves become considerably sharper with the increase of  $Wi_R$  and a

second overshoot in the birefringence is clearly apparent only at the highest  $Wi_R$ . With the increase of  $Wi_R$ , the polymer response time reduces (as can be seen from the shift of the temporal positions of these overshoots and undershoots toward shorter times) and the asymptotic birefringence monotonically decreases. Despite these similarities, in sharp contrast to the observations made with PS82, the long-time value of the transient birefringence in PS81 is always lower than the maximum in the first overshoot. Also, at high values of  $Wi_R$ , the orientation angle shows a distinct undershoot, followed by an overshoot and a second undershoot, which too become more intense with increasing  $Wi_R$ . There is a strong correlation in their temporal positions with that of the overshoot, undershoot and a second overshoot found in the birefringence data at the same  $Wi_R$ . Interestingly, the second undershoot in the orientation angle is clearly visible at a lower  $Wi_R$  before the second overshoot appears in the corresponding birefringence. At the highest  $Wi_R$ , the data for  $\chi$  versus  $t_e$  shows some ringing before reaching its long-time value,  $\chi_\infty$ . In similarity with the sample PS82, here too the conformational dynamics appear different below and above a transition Weissenberg number ( $Wi_R = 0.103$ , for PS81). At  $Wi_R > 0.103$ , the extremum in the undulations in both birefringence and orientation angle move faster to earlier times, and  $\chi_\infty$  approaches faster to  $\chi_\infty \sim 21^\circ$  at the highest  $Wi_R$ .

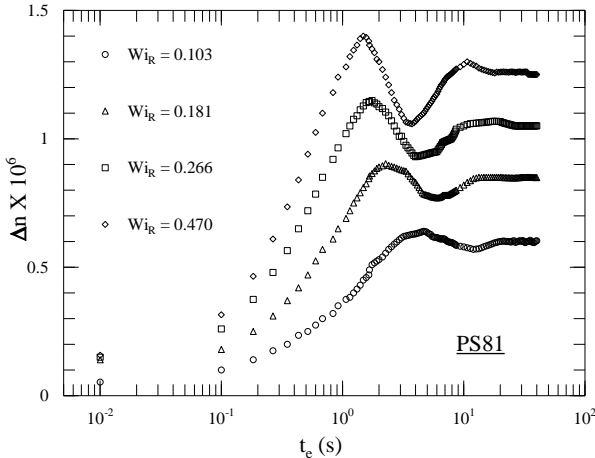


FIG. 18. Same as Fig. 17, but at higher Weissenberg numbers.

The dynamic evolution of the velocity-gradient components,  $\dot{\gamma}$  and  $\dot{\gamma}\lambda$  for the sample PS81 at the Weissenberg numbers corresponding to Figs. 17 to 20 are shown in Figs. 21 to 24, respectively. The flow-type parameter versus the evolution time,  $t_e$ , at the same values of  $Wi_R$ , extracted from these two results are depicted in Figs. 25

and 26. At the lowest rates of deformation, both measured components of the velocity-gradient,  $\dot{\gamma}$  (Fig. 21) and  $\dot{\gamma}\lambda$  (Fig. 23), (and hence  $\lambda$  in Fig. 25) remain almost constant over the entire evolution time of  $T = 30$  s, although there is a tendency of a slight undershoot at  $t_e \sim 4$  s in  $\dot{\gamma}\lambda$  curves. The impact of the changes in polymer configuration at these different Weissenberg numbers is more apparent on  $\dot{\gamma}\lambda$  and hence on  $\lambda$ , compared to the corresponding  $\dot{\gamma}$ . This is clearly seen from these figures where  $\dot{\gamma}$  approximately retains the Newtonian value,  $\dot{\gamma}_N$ , in time, but  $\dot{\gamma}\lambda$  and  $\lambda$  are higher than  $\dot{\gamma}_N\lambda_N$  and  $\lambda_N$ , respectively. At higher  $Wi_R$ , both  $\dot{\gamma}$  and  $\dot{\gamma}\lambda$  show an undershoot behavior at  $t_e \sim 4$  s before reaching their corresponding long-time values by  $t_e \sim 15$  s, except for the case of the highest deformation rate,  $Wi_R = 0.699$ , where  $\dot{\gamma}$  continues to increase (Fig. 22) and the curve for  $\dot{\gamma}\lambda$  has a higher asymptotic value than the rest of the curves in Fig. 24. The initial value of the flow-type parameter reduces from about 0.4 (Fig. 25) to about 0.1 (Fig. 26) with the increase of  $Wi_R$ , primarily because of the corresponding changes seen in the initial value of  $\dot{\gamma}\lambda$ . In contrast, we have noted that for both PS82 and PS81,  $\dot{\gamma}$  always “begins” with a value very close to the Newtonian-value,  $\dot{\gamma}_N$ . As seen for  $\dot{\gamma}$  and  $\dot{\gamma}\lambda$  versus  $t_e$  curves, the flow-type parameter for PS81 too undershoots at  $t_e \sim 4$  s. In similarity with the observations made for PS82, the asymptotic value of  $\lambda$  at the highest Weissenberg number reduces to  $\lambda_\infty \sim 0.1$ , and there is a clear-cut difference in the temporal behavior of the flow-parameters below and above a transition rate of flow-deformation,  $Wi_R = 0.103$ . Compared to PS82, the overall variation of magnitude of the flow-parameters over the total evolution time is less pronounced for PS81.

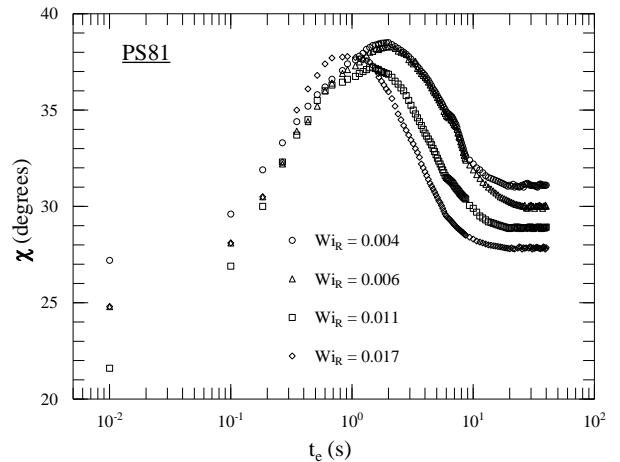


FIG. 19. Time-dependent orientation angle on inception of a two-roll mill flow for PS81 at several different values of measured steady-state  $Wi_R$ .

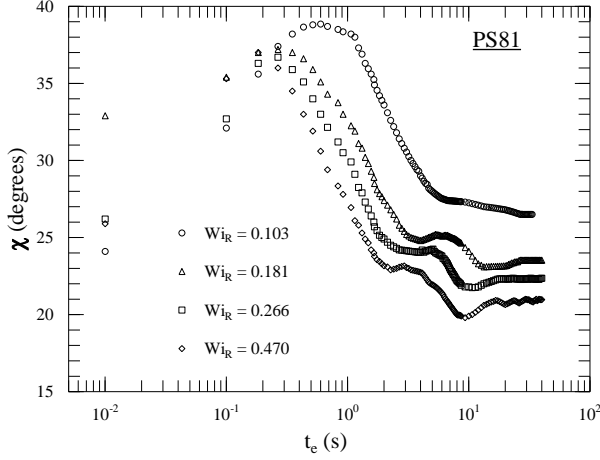


FIG. 20. Similar to Fig. 19, but at higher measured rates of flow-deformation,  $Wi_R = \dot{\gamma}\lambda^{1/2}\tau_R$ .

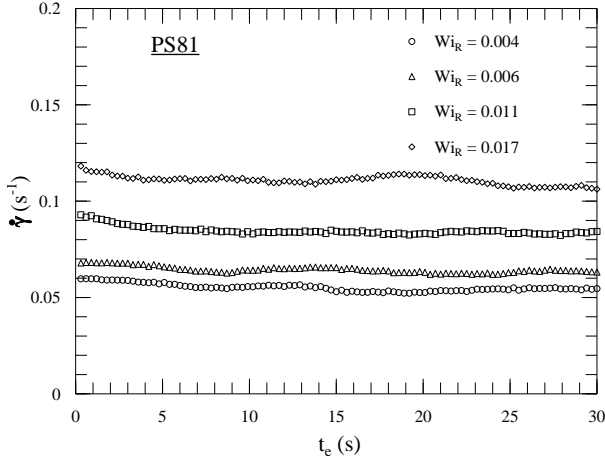


FIG. 21. Flow-induced changes in the evolution of velocity-gradient component,  $\dot{\gamma}$ , obtained from the exponential decay rate of the correlation functions at  $\phi = 0^\circ$  in start-up flow for PS81 and different measured steady-state Weissenberg numbers.

In general terms, the results for the solution PS2 (having about 13 entanglements per chain) shown in Figs. 27 to 30, is very similar to PS81 (also having  $N_e \sim 13$ ). In particular, the feature of the monotonic increase of birefringence to its asymptotic value at lowest  $Wi_R$  changes to that of the appearance of an overshoot, followed by an undershoot and another overshoot with the increased rate of deformation. In similarity with our observations

on the other two samples, here too all these undulations seem to appear earlier in time and their amplitudes increase with  $Wi_R$ . In contrast to PS82 and PS81, at highest rates of deformation, the asymptotic birefringence for PS2 in Fig. 28 is similar to the value at the first overshoot. In this case too, there is a critical Weissenberg number,  $Wi_R = 0.075$ , below which the evolution in both  $\Delta n$  and  $\chi$  is monotonic but above this number, they show undulations which become stronger as the Weissenberg number is augmented. Each undershoot (or overshoot) in the orientation angle curve is strongly correlated and a little shifted in time compared to the corresponding overshoot (or undershoot) in the birefringence curve. With the increase of  $Wi_R$ , here too the asymptotic birefringence gradually increase and the asymptotic orientation angle,  $\chi_\infty$ , gradually decrease. At the highest  $Wi_R$ ,  $\chi_\infty \sim 18.5^\circ$ , in Fig. 30. The prime difference in this case, compared to PS81, is that the magnitude of birefringence at the second overshoot is similar to the first overshoot and the asymptotic value.

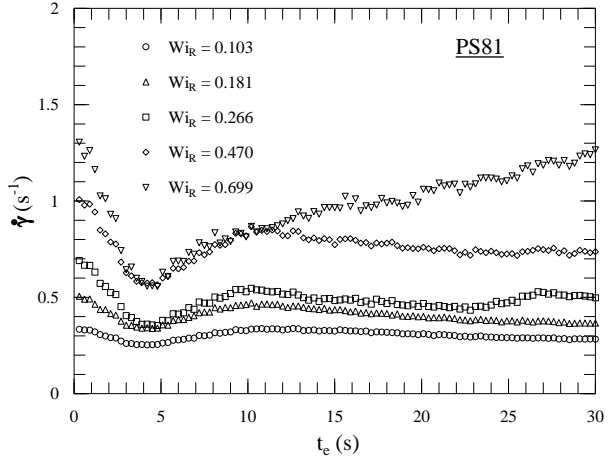


FIG. 22. Similar to Fig. 21, but for higher values of  $Wi_R$ .

As shown in Figs. 31 to 36, the characteristic evolution of the measured flow-parameters for PS2 is, again, extremely similar to that for PS81 (which has similar  $N_e \sim 13$ ), but is very different from that seen in PS82 ( $N_e \sim 7$ ). Here too  $\dot{\gamma}\lambda$  and hence  $\lambda$  seems to be much more sensitive than  $\dot{\gamma}$  to the changes in the polymer configuration in that their initial values are always different than that expected with a Newtonian fluid, which is not the case with  $\dot{\gamma}$ . Similar to PS81, the polymer-induced variation in the magnitude of flow-parameters for PS2 over the entire period of evolution time is not as pronounced as seen for PS82. The small undershoots at  $t_e \sim 4$  s present in  $\dot{\gamma}\lambda$  versus  $t_e$  (s) curves at all Weissenberg

numbers and also in  $\dot{\gamma}$  versus  $t_e$  curves at intermediate and high  $Wi_R$  almost cancel each other in  $\lambda$  versus  $t_e$  results, which are derived from the division of these two data sets. If at all, there is a little overshoot present in  $\lambda$  versus  $t_e$  curves at the similar evolution time  $t_e \sim 4$  s for  $0.151 \leq Wi_R \leq 0.236$ . The asymptotic limit of the flow-parameters are reached much earlier than  $t_e \sim 15$  s. Since the overall variation of the flow-parameters over the entire evolution time is not too pronounced for PS2 for any Weissenberg number, the changes in their transient evolution below and above the transition Weissenberg number,  $Wi_R = 0.075$ , is not too appreciably noticed here, except for the case of flow-type parameters in Figs. 35 and 36.

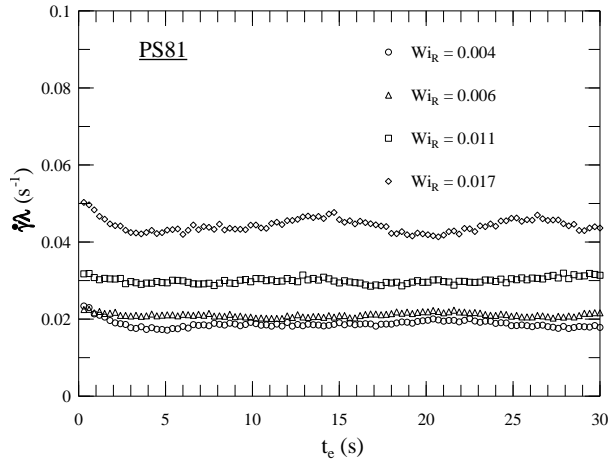


FIG. 23. Transient velocity-gradient component,  $\dot{\gamma}\lambda$ , for PS81, versus evolution time,  $t_e$ , for inception of a two-roll mill flow at several measured steady-state  $Wi_R = \dot{\gamma}\lambda^{1/2}\tau_R$ .

#### IV. DISCUSSION OF RESULTS

Turning back to the results for the three entangled samples, the prime important feature to note is that the dynamical response of the polymer systems, PS81 and PS2, with a similar number of entanglements per chain appears to be very much similar, even though they have quite different concentrations,  $c$ , and molecular weights,  $M_w$  (see, Table I). On the other hand, the dynamics is very different from these two for the sample PS82, which has a different number entanglements per chain. This should be expected, based upon the scaling ideas associated with reptation modelling, provided we stay away from chain-stretching. In the limit of high  $Wi_R$ , the DEMG version [3,4] of the reptation model, used in Part I, predicts a saturation of the dimensionless steady-state birefringence of  $\sim n_t/N_e$  corresponding to a maximum

chain-extension ratio of  $\sim \sqrt{n_t/N_e}$ . As in Part I, we first non-dimensionalize the asymptotic values of the birefringence shown in Figs. 8, 18, and 28 at the highest  $Wi_R$  by scaling them with the birefringence  $CG_N^0$  (obtained by using the stress-optical law) that would be present at a stress level equal to the plateau modulus,  $G_N^0$ . The values used for the stress-optical coefficient,  $C$ , and the plateau modulus are same as in Part I [12]. Comparing these values to the DEMG predictions given above, we see that the experimentally observed maximum asymptotic chain-extension for these samples are  $\sim 44.04\%$  for PS82,  $\sim 6.63\%$  for PS81, and  $\sim 11.04\%$  for PS2. This is a clear indication of the fact that we are quite away from the chain-stretching behavior. The impact of the changes in the polymer conformational dynamics, as depicted by the time-evolution of the measured components of velocity-gradients,  $\dot{\gamma}$ , and  $\dot{\gamma}\lambda$ , and hence the flow-type parameter,  $\lambda$ , too is also extremely similar for PS81 and PS2, and this dynamical behavior is very different from that seen in the case of PS82.

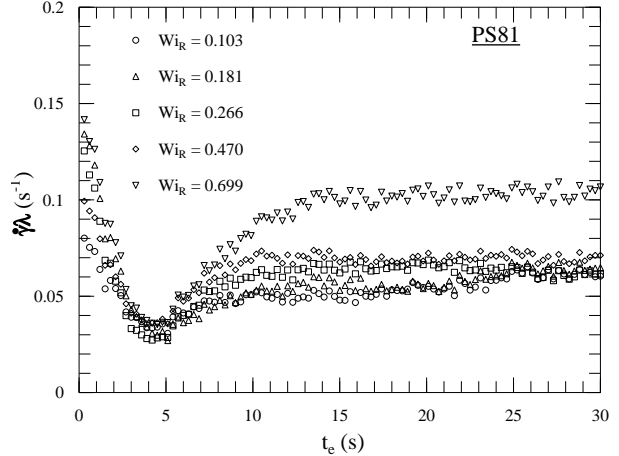


FIG. 24. Same as in Fig. 23, but at higher  $Wi_R$ .

As we have mentioned before, the occurrence of an overshoot in the birefringence and an associated undershoot in the orientation angle at a slightly shifted time, have been observed earlier for the start-up of a simple shear flow ( $\lambda = 0$ ) [7,8], as well as for the start-up flow with a little more extensional character ( $\lambda = 0.019$ ) in a two-roll mill [18]. For simple shear flows, the onset of the overshoot in the first normal stress difference (birefringence) occurs at  $\dot{\gamma}_N\tau_R \sim 0.4 - 0.7$  [4,19]. The onset of the birefringence overshoot in our experiments occur at the measured Weissenberg numbers that are very different from sample to sample, namely, at  $Wi_R \sim 0.144$  for PS82,  $Wi_R \sim 0.017$  for PS81, and at  $Wi_R \sim 0.027$

for PS2. These numbers correspond to  $\dot{\gamma}_N \tau_R \sim 0.5$  for the less entangled sample, PS82, and  $\dot{\gamma}_N \tau_R \sim 0.3$  for the other two more entangled samples, PS81 and PS2, which are in the same ballpark with the earlier results [4,18,19].

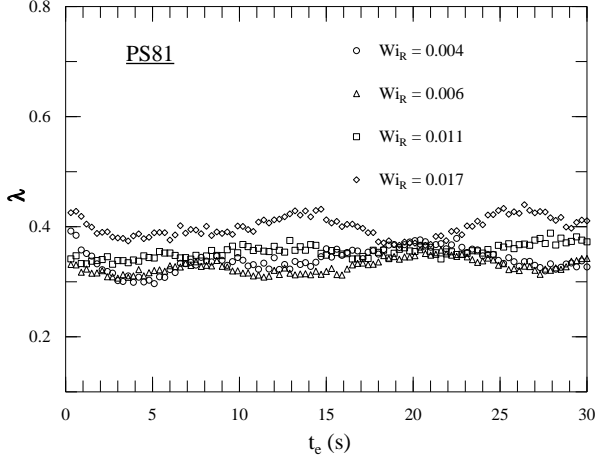


FIG. 25. Time-dependence of the flow-type parameter,  $\lambda$ , obtained via point-by-point division of the corresponding data for  $\dot{\gamma}\lambda$  by  $\dot{\gamma}$  for PS81 at different measured steady values of  $Wi_R$ .

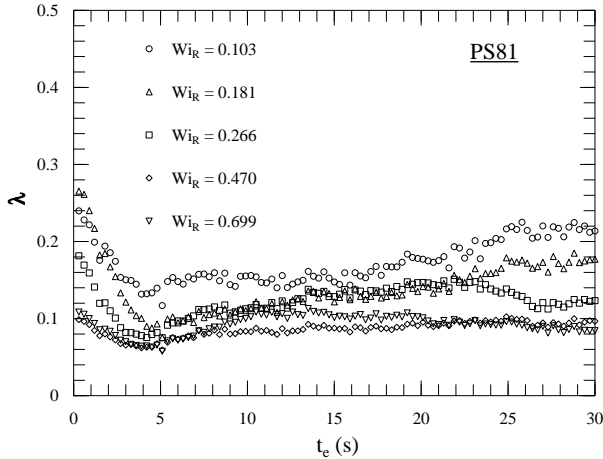


FIG. 26. Similar to Fig. 25, but at higher measured rates of deformation,  $Wi_R = \dot{\gamma}\lambda^{1/2}\tau_R$ .

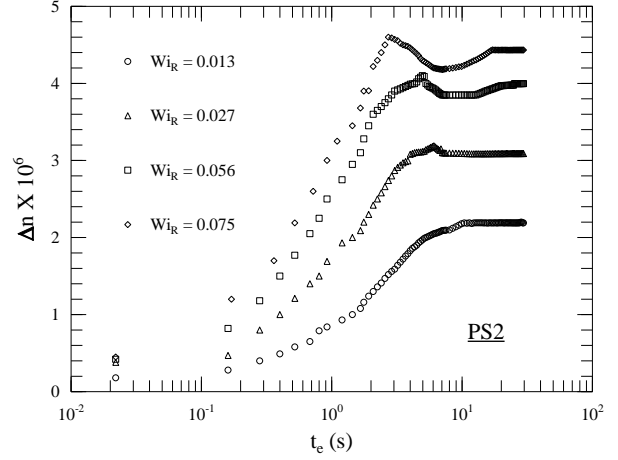


FIG. 27. Birefringence for PS2 solution in start-up flows at different measured dimensionless rates of flow-deformation,  $Wi_R = \dot{\gamma}\lambda^{1/2}\tau_R$ .

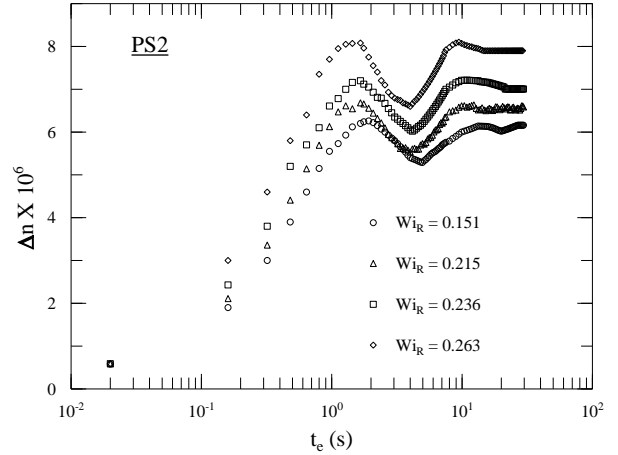


FIG. 28. Same as Fig. 27, but at higher measured  $Wi_R = \dot{\gamma}\lambda^{1/2}\tau_R$ .

Here, too the number of entanglements per chain seem to have an important role to play. We note that the birefringence overshoot for the inception of a simple shear flow have also been predicted using the Doi-Edwards reptation model with chain-stretching [4], although the undershoot in the orientation angle was not predicted. In this work, as well as in prior work [7,8,11,18] on polymers, the undershoot behavior in the orientation angle seem to be very much correlated in time with the overshoot behavior in the birefringence. According to the

model, the transient nature of chain-stretching in a simple shear is responsible for the overshoots. On the basis of the DEMG model [3,4], it was speculated in earlier work [8,11] from our laboratory that “tube-dilation” may be responsible for such an effect. In simple terms, this means that a flow-deformation induced decrease in the number of entanglements per chain (and hence the dilation in the tube-radius) takes place on a slower time-scale than over which the polymer orients. This faster orientation would allow polymer to over-orient (and thereby show an undershoot in the transient orientation angle) and then relax to its asymptotic value as  $N_e$  is decreased. From Figs. 16, 26 and 36, at the highest Weissenberg numbers, we get  $\lambda_\infty \sim 0.10$  for PS82 and PS81, and  $\lambda_\infty \sim 0.11$  for PS2. These estimate  $\chi_\infty \sim 17.5^\circ$  for PS82 and PS81, and  $\chi_\infty \sim 18.3^\circ$  for PS2, but the experimental results at the highest  $Wi_R$ , as can be seen in Figs. 10, 20 and 30 are  $\chi_\infty \sim 14.8^\circ$  (PS82),  $\chi_\infty \sim 21^\circ$  (PS81), and  $\chi_\infty \sim 18.5^\circ$  (PS2), respectively.

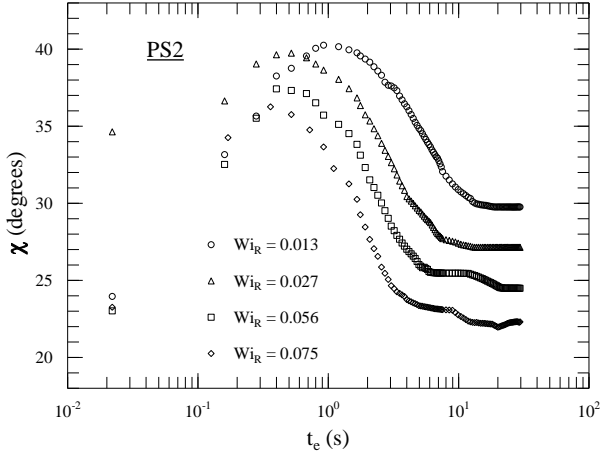


FIG. 29. Plot of the dynamic evolution of orientation angle on inception of steady-flows for PS2 at several steady-state values of measured  $Wi_R$ .

The velocity-gradient components measured via dynamic light scattering experiments show that there is a significant amount of flow-modification by the polymers relative to the otherwise Newtonian-value. The flow-modification appears to be very strong for all polystyrene samples (see, Table II), but the evolution of the flow-parameters over the total duration  $T$  of our transient experiments show most dramatic changes for the sample with the lowest entanglements per chain. In comparison, this effect is rather weak for PS81 and PS2, both with  $N_e \sim 13$ . We have noted that the velocity-gradient component,  $\dot{\gamma}\lambda$ , for the perpendicular orientation of the two-roll mill and hence the flow-type parameter,  $\lambda$ , is

much more sensitive to the polymer induced changes in the flow than the other velocity-gradient component,  $\dot{\gamma}$ . At the lowest  $Wi_R$ , the values of the flow-type parameters for all three samples, deduced from the corresponding  $\dot{\gamma}\lambda$  and  $\dot{\gamma}$  measurements, are consistently higher than that expected for a Newtonian fluid. This finding is also consistent with that in our steady-state experiments [12] on the same polymeric fluids. We note that an increase in the value of flow-type parameter in the vicinity of the stagnation-point of the two-roll mill, relative to the Newtonian-value at small  $Wi_R$  was not observed by Wang *et al.* [10] because we explored the range of measured  $Wi_R$  much lower than their study. This is the only earlier experiment, that we are aware of, which has performed simultaneous TCFB and DLS measurements on entangled polymers subjected to inception of two-roll mill flows. On the other hand, recent numerical simulations, using a vector approximation [6] of the DEMG reptation model, by Remmelgas *et al.* [20] indeed predicted the same result for entangled polymeric fluids in the same configuration ( $\lambda_N = 0.1501$ ) of the two-roll mill. Ongoing experiments and theoretical work in our laboratory are intended to look into this important issue.

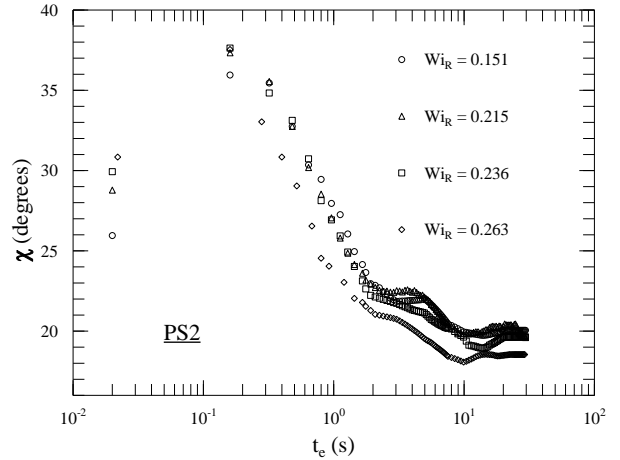


FIG. 30. Same as Fig. 29, but at higher  $Wi_R = \dot{\gamma}\lambda^{1/2}\tau_R$ .

For all cases studied here, as the flow evolve to high  $Wi_R$ , the measured values of both the velocity-gradient,  $\dot{\gamma}$ , and the flow-type parameter,  $\lambda$ , and hence the strain-rate,  $\dot{\gamma}\sqrt{\lambda}$ , have reduced relative to the velocity-field for a Newtonian fluid. The reduction of the extensional strength of the flow as well as the strain-rate in the neighborhood of the stagnation-point was observed for dilute polymers [17,21] too for which it has been shown theoretically [17,22], using nonlinear dumbbell models [26], to be related to the strain-rate hardening [23] of the exten-



sional viscosity of these fluids. Obviously, a completely different methodology has to be responsible for the entangled polymeric fluids, since they show a strain-rate softening of the extensional viscosity. The recent work of Remmelgas *et al.* [20] have, in fact, predicted the decrease in the rate of strain for entangled polymeric fluids at the stagnation-point, in similarity with our experiments. This decrease was shown to result from the effect of shear thinning viscosity in the flow close to the rollers making the momentum transfer to the region between the rollers less efficient.

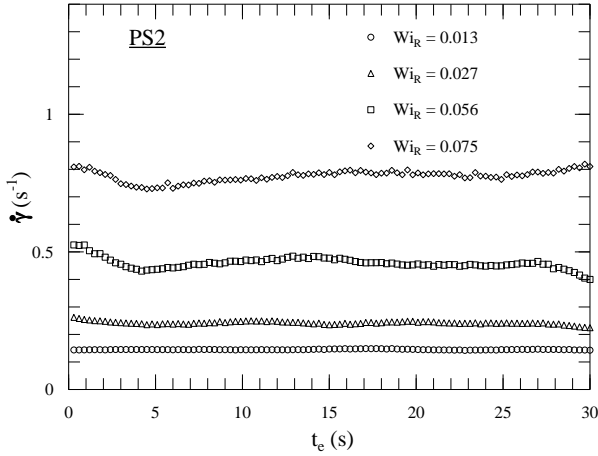


FIG. 31. Transient  $\dot{\gamma}$  versus  $t_e$  in start-up of steady-flows for PS2 at different measured  $Wi_R$ .

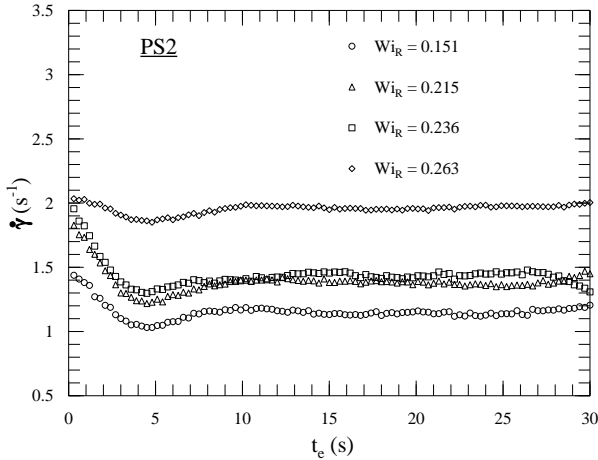


FIG. 32. Same as Fig. 31, but at higher measured values  $Wi_R = \dot{\gamma}\lambda^{1/2}\tau_R$ .

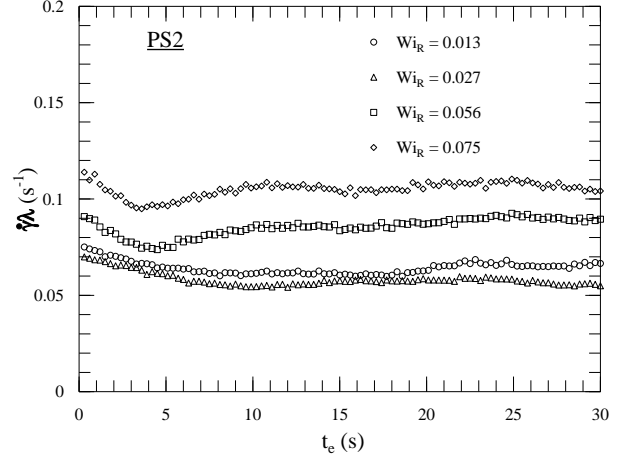


FIG. 33. Transient velocity-gradient component,  $\dot{\gamma}\lambda$ , versus  $t_e$  for PS2 with the two-roll mill orientation  $\phi = 90^\circ$ , and at different  $Wi_R$ .

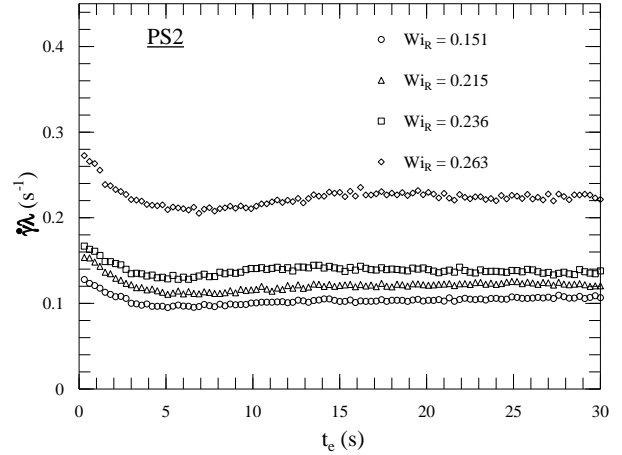


FIG. 34. Same as Fig. 32, but at higher measured values of Weissenberg numbers.

#### A. Comparison of dynamics at similar $Wi_R$

We will now compare the results for the three entangled solutions at the similar values of the measured Weissenberg numbers, namely,  $Wi_R = 0.284$ ,  $0.266$ , and  $0.263$  for PS82, PS81 and PS2, respectively. Fig. 37 shows the birefringence traces versus  $t_e$ , where the birefringence for each sample is normalized by the asymptotic value, for the purpose of comparison. The corresponding curves for

the evolution of the orientation angle,  $\chi$ , and the flow-parameters,  $\dot{\gamma}$ ,  $\dot{\gamma}\lambda$  and  $\lambda$  are shown in Figs. 38 to 41.

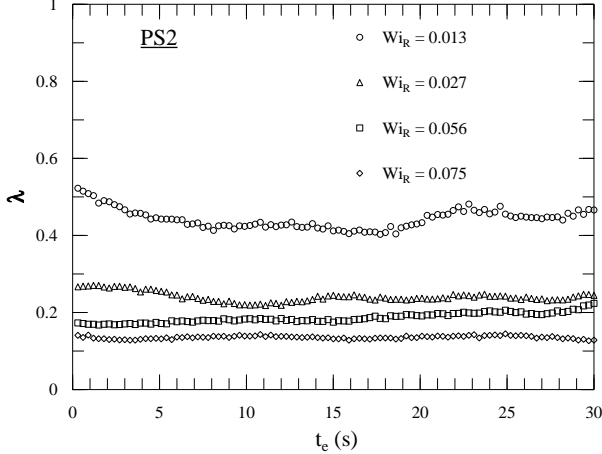


FIG. 35. Flow-induced changes in flow-type parameter,  $\lambda$ , versus  $t_e$  for PS2 at different measured rates of flow-deformations,  $Wi_R = \dot{\gamma}\lambda^{1/2}\tau_R$ .

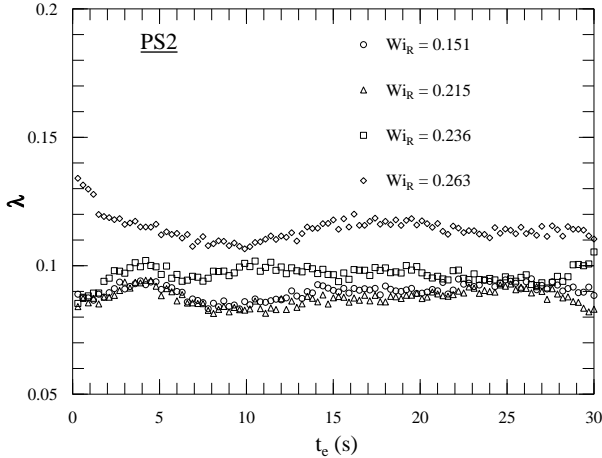


FIG. 36. Same as Fig. 35, but at higher measured  $Wi_R$ .

One of the prime important results of this study, that the evolution dynamics of the polymer microstructure as well as its impact on the flow-field is very much dependent on the number of entanglements per chain for the polymers irrespective of the values of  $M_w$  and  $c$ , become very clear from the comparisons of these figures. In particular, the normalized birefringence in Fig. 37 shows an overshoot, followed by an undershoot and a second over-

shoot at exactly similar times for both PS81 and PS2; even the magnitude of these undulations are very similar when normalized with the asymptotic value, and the first overshoot is higher than the asymptotic value. In contrast, the normalized birefringence for PS82 does not show a clear second overshoot at similar rates of flow-deformation; the times at which the overshoot and the following undershoot appear for the birefringence of PS82 are, again, very different from that seen with the other two samples, and also, the asymptotic value in this case is much higher than the overshoot. Similarly, the orientation angles (Fig. 38) for PS81 and PS2 shows an undershoot behavior, followed by an overshoot and a second undershoot (deeper than the first one), each of which appear at a slightly later time than the corresponding undulations seen in the birefringence curves. These strong correlation in their appearance directly indicates that same microscopic dynamics must be responsible for both of these observations. Thus, the orientation angle traces are very similar for these two samples having similar  $N_e$  but is very different for PS2, where after overcoming the residual glass-birefringence, it almost monotonically decreases to the asymptotic value without showing any undershoot behavior. The similarity in the shape of the curves for the measured flow-parameters versus evolution time too are very surprising. We note that the undershoot in flow-parameters (at  $t_e \sim 4$  s for PS81 and PS2, and at  $t_e \sim 12$  s for PS82) is very directly correlated with the first overshoot in the birefringence or the first undershoot in the orientation angle (appearing at  $t_e \sim 2$  s for PS81 and PS2, and at  $t_e \sim 9$  s for PS82). The intensity of these undulations in the flow-parameters are also strongly correlated with the intensity of the corresponding undulations in the birefringence and orientation angle. Also, the oscillations are always found to be weaker in the case of PS82. These results, again, very clearly emphasize that the coupled dynamics of the flow and the polymer configuration are invariant to changes in the concentration and/or molecular weight, provided that the same value of the number of entanglements per chain is maintained.

At these rates of deformation, by comparing the measured and the Newtonian-values of the Weissenberg numbers from Table II for the three polymeric fluids, we note that the flow-induced reduction in Weissenberg number or the strain-rate is similar for PS82 and PS2. Thus, we may expect similar values of the asymptotic orientation angle and the asymptotic stretch of these two polymers. In Fig. 38, we indeed see a similar long-time value of the orientation angle for these two samples. As noted earlier, the DEMG reptation model predicts that at very high Weissenberg numbers, the polymer chains are extended to the maximum chain-extension ratio of  $\sqrt{n_t/N_e}$ , and the corresponding steady-state value of dimensionless birefringence is  $\sim n_t/N_e$ . By comparing the asymptotic value of the dimensionless birefringence,  $\Delta n/CG_N^0$ , for

PS82 (Fig. 7), PS81 (Fig. 18), and PS2 (Fig. 28) with the aforesaid steady-state value, we see that compared to the fully extended state, at these similar Weissenberg numbers, the polymer chains are stretched to about 10.39%, 5.62%, and 11.04% for PS82, PS81 and PS2, respectively. The similar extensibility witnessed for PS82 and PS2 is consistent with the similar flow-induced reduction of the measured Weissenberg number compared to the Newtonian-value for these two solutions. Between the fluids with the similar high molecular weight polystyrene, PS82 and PS81 (refer Table I), the dilute (and hence the less entangled) solution, PS82, has higher molecular weight of the chain-segments between entanglements and hence an increased intrinsic extensibility in this case could be expected. This might be an added reason, other than the polymer-modified flow as discussed above, for PS82 showing a higher fractional chain-extension compare to PS81 at the similar  $Wi_R$ . We note that since the curves for  $\lambda$  versus  $t_e$  (Fig. 41) are approximately close to each other for the three polystyrene fluids, in order to keep the measured Weissenberg number similar, the velocity-gradient curve,  $\dot{\gamma}$  versus  $t_e$ , in Fig. 39 (and hence  $\dot{\gamma}\lambda$  versus  $t_e$  in Fig. 40) is higher for PS2 than that for the other two samples in the same ratio as the longest Rouse relaxation time,  $\tau_R$ , for PS2 is lower than  $\tau_R$  for PS81 and PS82.

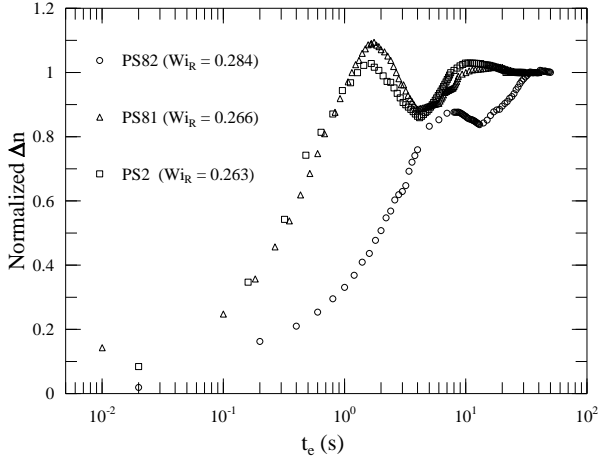


FIG. 37. Plot of the time-evolution of birefringence,  $\Delta n$ , normalized with the corresponding asymptotic values, for all three polystyrene samples on inception of steady-flows at similar measured steady-state  $Wi_R$ .

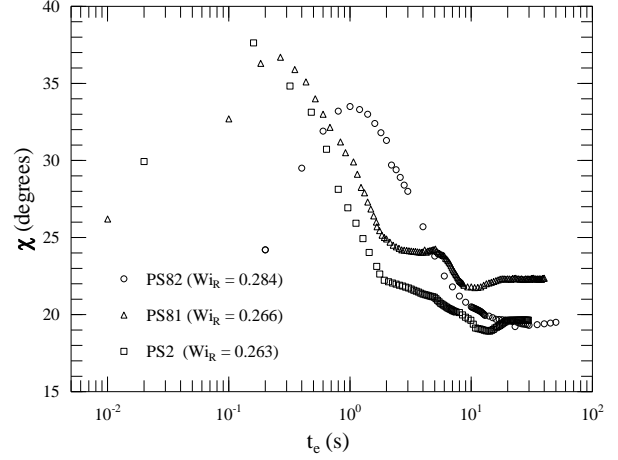


FIG. 38. Same as Fig. 37, but for the orientation angle,  $\chi$ .

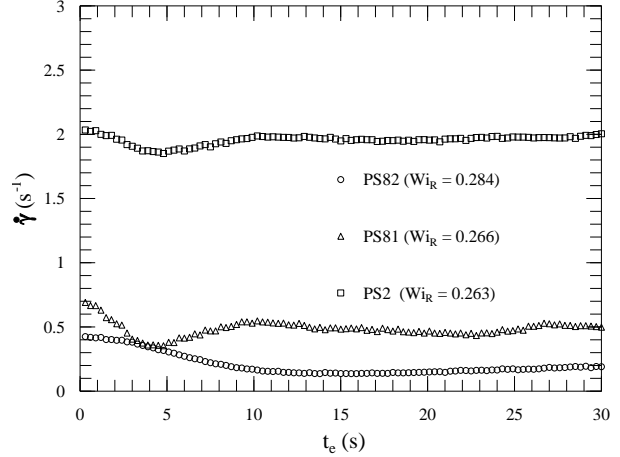


FIG. 39. Transient evolution of the velocity-gradient,  $\dot{\gamma}$ , for all three polystyrene samples at similar measured  $Wi_R$ .

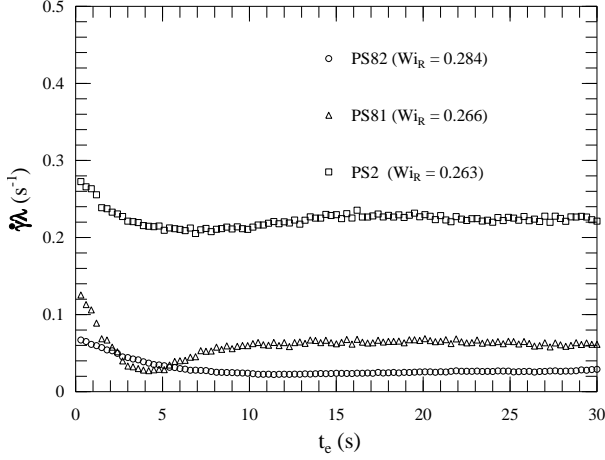


FIG. 40. Same as Fig. 39, but for a different velocity-gradient component,  $\dot{\gamma}\lambda$ .

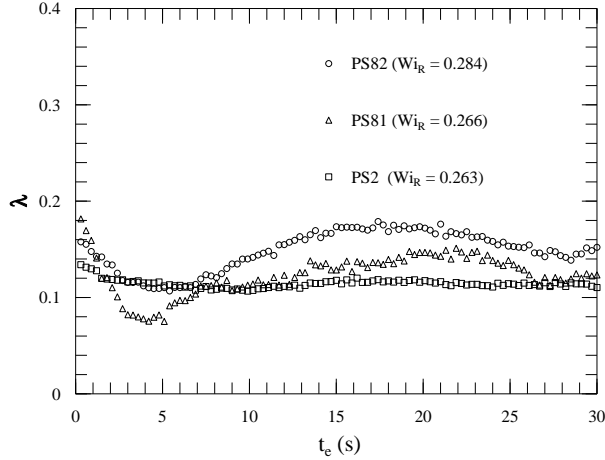


FIG. 41. Dynamic evolution of the flow-type parameter,  $\lambda$ , on inception of steady-flows for all three polymeric fluids at similar measured  $Wi_R$ .

### B. Characteristic strains for inception of flow

Following the lead of the work by Geffroy *et al.* [18], we have measured the total strain at the peak of the birefringence overshoot for the three entangled polystyrene solutions at several different rates of deformation. The characteristic strain at the peak of the stress (or birefringence) overshoot was found to be an useful parameter to determine the transition from linear to non-linear vis-

coelastic behavior of polymers [4,18,19,24]. It was shown in the past that the strain to reach the birefringence overshoot are nearly constant at low rates of deformation, but it increases by several orders of magnitude at high rates for both simple shear flow [25] and extension-dominated flows [18,24], signifying a transition from linear to non-linear viscoelastic behavior. For the simple shear flow, this constant was proposed [19] to be about unity, independent of the polymer molecular weight and this was experimentally verified [19,25] too. For extensional flows, on the other hand, this onset strain was found [18,24] to be  $\sim 0.7$ . It was proposed [19] that irrespective of the polymer type and/or molecular weight, the onset of the non-linear viscoelastic behavior should begin near  $\dot{\gamma}_N \tau_R \sim 1$ , which, in this particular geometry of the two-roll mill ( $\lambda_N = 0.1501$ ), turns out to be  $(Wi_R)_N = \dot{\gamma}_N \sqrt{\lambda_N} \tau_R \sim 0.4$ , where  $(Wi_R)_N$  is the Weissenberg number based on the Newtonian values of the velocity-gradient component,  $\dot{\gamma}_N$ , the flow-type parameter,  $\lambda_N$ , and the longest Rouse relaxation time,  $\tau_R$ . In previous work with extension-dominated flows [18,24], the stain at the overshoot was calculated as the time to reach the overshoot times the Newtonian strain-rate, that is  $\dot{\gamma}_N \sqrt{\lambda_N} t_p$ .

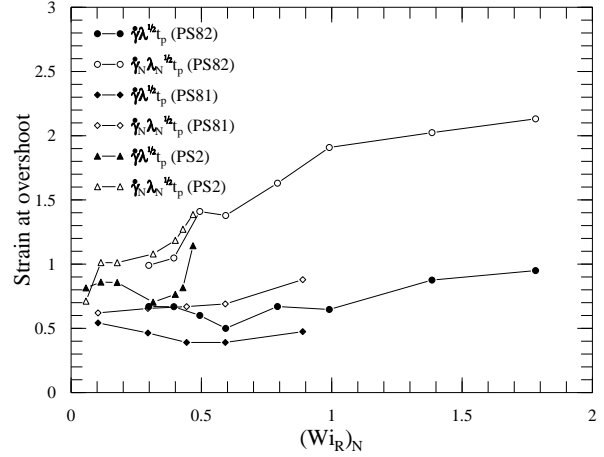


FIG. 42. Strain at the overshoot of birefringence against the  $(Wi_R)_N = \dot{\gamma}_N \lambda_N^{1/2} \tau_R$  for all three polystyrene samples.

In Fig. 42, we have presented our results for the Newtonian as well as the measured value of the peak-strain at the overshoot for the three entangled polystyrene fluids as a function of  $(Wi_R)_N$ , in order to simplify the comparisons with the earlier results. In similarity with the earlier observations [18,24], at the lowest rate of flow-deformation, the Newtonian-strain at the birefringence overshoot is  $\dot{\gamma}_N \sqrt{\lambda_N} t_p \sim 0.7$ , and its value increases with the deformation rate. Interestingly, this increase with

the rate of deformation is similar for samples PS82 and PS2, both having  $N_e \sim 13$ . At  $(Wi_R)_N \sim 0.4$ , a modest change in slope in  $\dot{\gamma}_N \sqrt{\lambda_N t_p}$  is also apparent particularly for these two samples. In contrast, the measured value,  $\dot{\gamma} \sqrt{\lambda t_p}$ , of the strain at the overshoot peak of birefringence, although “begins” at a value (viz., 0.5 – 0.7) that is similar to 0.7, it shows an initially decreasing and then increasing trend with the increase of the rate of deformation for all three polystyrene samples. The change in the trend occurs at  $(Wi_R)_N$  between 0.3 and 0.6 for all three fluids, which is again similar to the proposed value of 0.4. The distinct difference between the curves for  $\dot{\gamma}_N \sqrt{\lambda_N t_p}$  and  $\dot{\gamma} \sqrt{\lambda t_p}$  is, again, indicative of the fact that the changes in the polymer conformation and the flow-deformation are crucially inter-twined.

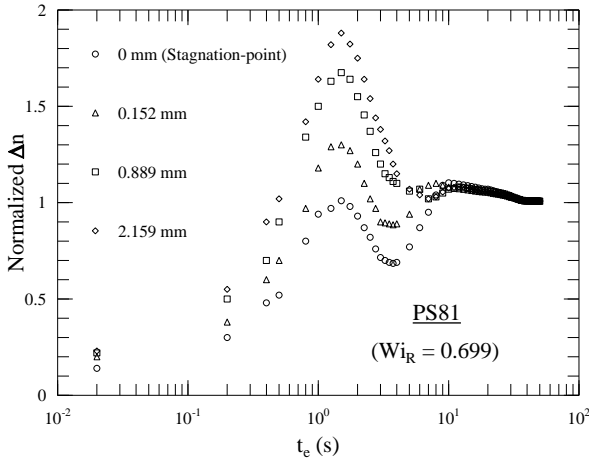


FIG. 43. Transient evolution of birefringence, normalized with the corresponding asymptotic values, for the same sample, PS81, at the same measured  $Wi_R = 0.699$ , but at several different points across the gap between the stagnation-point and the roller surface of the two-roll mill.

### C. Measurements at different positions within the flow

It is understandable that the overall flow in a two-roll mill will be very complicated and the stagnation region in which we perform our birefringence as well as flow measurements is a very small and special region of the entire flow where the flow can be approximated by the uniform and homogeneous form given by Eqn. (1), for both Newtonian and viscoelastic fluids. Hence, to try to measure and interpret the polymer conformation, the flow kinematics and/or their coupling in any region of the flow other than the stagnation would be an extremely difficult experimental task. Earlier numerical simulation results

(using the Chilcott-Rallison model [26] for dilute polymeric solutions [22], and the vector model [20] for the entangled polymer solutions) for the present configuration of the two-roll mill (i.e., with  $\lambda_N = 0.1501$ ), had shown that at a constant rate of imposed flow-deformation, the extensional character of the flow (i.e., the value of  $\lambda$ ) as well as the rate of strain,  $\dot{\gamma} \sqrt{\lambda}$ , reduce compared to their Newtonian-value,  $\lambda_N$ , and  $\dot{\gamma}_N \sqrt{\lambda_N}$ , respectively, (or the flow becomes more shear-like) in the region close to the roller surface. In fact for the entangled fluids [20], the rate of strain in the gap between the rollers smoothly changes its value from a minimum at the stagnation-point to a maximum at the roller surface. The difference between the minimum and the maximum could be as high as three to four times depending on the concentration of the sample.

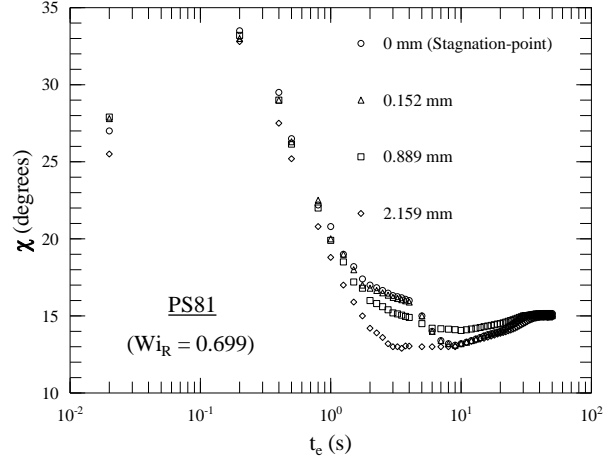


FIG. 44. Same as Fig. 43, but for inception of orientation angle,  $\chi$ .

We have attempted to measure the birefringence and the flow-parameters at different points in the two-roll mill flow from the stagnation-point to the roller-surface when the two-roll mill is orientated along the  $y$  axis in Fig. 2, i.e., when  $\phi = 90^\circ$ . The flow measurements are also performed for the other orientation of the two-roll mill, i.e., when it is orientated along  $x$  axis ( $\phi = 0^\circ$ ). It is intrinsic to our set-up that the two-roll mill can be rotated only about the central stagnation-point. This restricts us to measure only one velocity-gradient component at different points along the  $x$  and  $y$  axes when the flow-cell is orientated along the same directions. At the stagnation-point these two velocity-gradient components are just  $\dot{\gamma}$  and  $\dot{\gamma} \lambda$ , respectively. In these attempts, we have assumed that the flow at different positions along these two axes, to a first approximation, can still be described by Eqn. (1), so that the process of measuring the

velocity-gradient parameters via dynamic light scattering is still valid. Although this has not been rigorously verified, pending the availability of a more detailed calculation for measuring the velocity-gradient parameters at different points in the flow, we can still use the same DLS technique to get an approximate picture of the flow kinematics. The distance from the stagnation-point to the surface of the rollers for the present configuration of the two-roll mill is 4.22 mm, but the gear assembly attached in front of the two-roll mill obstructs the beam to go through the sample-cell beyond a distance of 1.3 mm from the stagnation-point when the flow-cell is orientated along  $y$  axis. This restriction does not apply when the two-roll mill is rotated along  $x$  axis.

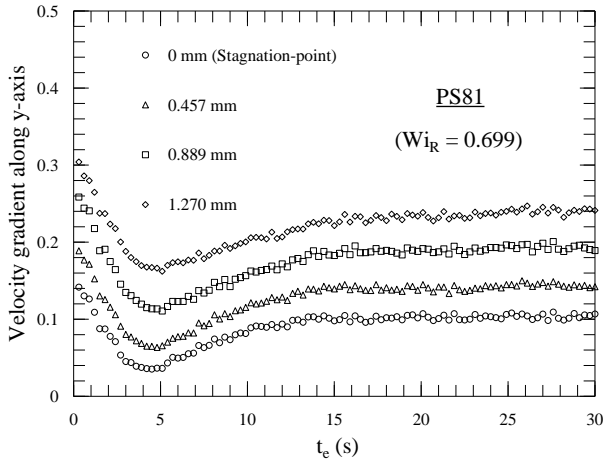


FIG. 45. Transient evolution of the velocity-gradient component at several different points along  $y$  axis of Fig. 1 for sample, PS81, at the measured Weissenberg number,  $Wi_R = 0.699$ , and the two-roll mill orientation,  $\phi = 90^\circ$ .

Fig. 43 and 44 show the temporal-evolution of the birefringence (scaled with the corresponding asymptotic value), and the orientation angle at four different points along the  $y$  axis on inception of flow to a measured Weissenberg number of 0.699 for the polystyrene fluid PS81. The birefringence at the stagnation-point shows a very distinct overshoot and undershoot behavior before reaching the asymptotic value, which is higher than the peak overshoot. This is a characteristic feature shown by PS81 when subjected to extension-dominated flows, as we have noticed before in Fig. 18. As one approaches closer to the roller-surface from the stagnation-point, the strength of the overshoot increases but the undershoot diminishes so that we finally obtain a birefringence curve with a single peak and a slight undershoot measured at 2.159 mm away from the stagnation-point towards the surface of the rollers. Before the reaching the asymp-

totic value, the temporal-dependence of the orientation angle also exhibits a transition from a distinct undershoot behavior at stagnation-point and in the region close to it, characteristic of an extension-dominated flow, to a smaller and wider undershoot behavior quite away from the stagnation-point, characteristic of a more shear-like flow. This confirms the theoretical findings [20,22], as discussed above. The different curves for the orientation angle versus evolution time exhibit most differences from each other in the time-period  $t_e = 0.7 \text{ s} - 30 \text{ s}$ , which is shifted in time from the time-period  $t_e = 0.2 \text{ s} - 10 \text{ s}$ , over which the corresponding birefringence curves show most differences from each other. This, again, is consistent with our earlier observations. It is important to note from Fig. 44, that at the same measured  $Wi_R$  the polymer chains are asymptotically orientated to the same angle,  $\chi_\infty \sim 15^\circ$ , at different points studied within the gap between the rollers.

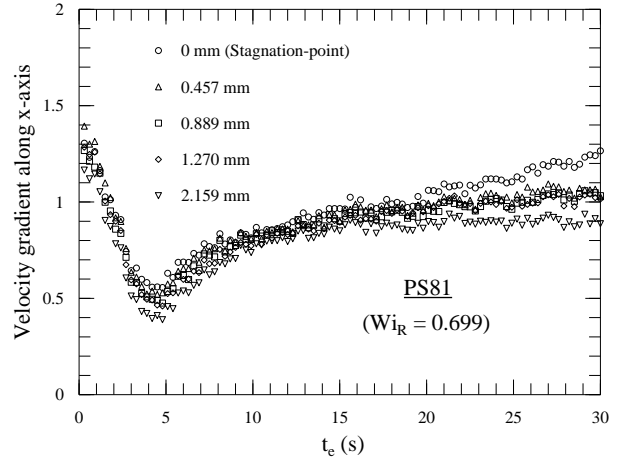


FIG. 46. Same as Fig. 45, but along  $x$  axis of Fig. 1 and 2, and  $\phi = 0^\circ$ .

The time-dependent velocity-gradient component along  $y$  axis for the inception of the same flow is depicted in Fig. 45. As noted before, at the stagnation-point, this parameter is simply  $\dot{\gamma}\lambda$ , which already shows the impact of the polymer induced flow-modification even at the first point of our measurement, i.e., as early as  $t_e = 0.3 \text{ s}$ , where its measured value is shown to be lower than the Newtonian-value of 0.2. The temporal behavior of this component at different positions along  $y$  axis, for  $\phi = 90^\circ$ , is surprisingly similar in shape to that of  $\dot{\gamma}\lambda$ . In particular, all of them “begin” with an initial higher value, pass smoothly through a minimum and again increase to reach the asymptotic value (which is lower than the initial value) as early as  $t_e \sim 15 \text{ s}$ . This component of the velocity-gradient tensor increases in magnitude when

approached towards the surface of the rollers from the stagnation-point. In sharp contrast to this, the component along  $x$  axis, when  $\phi = 0^\circ$ , does not change much between the two rollers. This is clearly shown in Fig. 46, where the different curves almost overlap on to each other until about  $t_e = 15$  s, beyond which the asymptotic value is reached faster in time in the region closer to the roller-surface, compared to that in the stagnation-point, where even at  $t_e = 30$  s, this component of velocity-gradient still shows an increasing trend. A closer look at the differences among these curves indicates that there is a decreasing trend in the value of this velocity-gradient component away from the stagnation-point at each instant of time during the flow evolution. This behavior is opposite to what is seen in Fig. 45. Interestingly, for all the curves shown in Figs. 45 and 46, the time at which the minimum of the undershoot is reached is almost constant,  $t_e \sim 4$  s. Similarly, the peak of the birefringence for all the curves occurs at  $t_e \sim 2$  s, and these two times are strongly correlated to each other. As we have noted before, these times are direct functions of the Weissenberg number of the flow and the molecular characteristics of the polymer, both of which are held fixed in this case. These observations are qualitatively in a very close agreement with that found using the vector model [6] by Remmelgas *et al.* [20] for the start-up of two-roll mill flows for entangled polymeric solutions. It is important to note that given the inherent difficulty of our set-up to measure the other velocity-gradient components corresponding to Figs. 45 and 46, a critical comparison to the findings of the above model on the flow in the gap between the rollers, discussed above, is impossible. Nevertheless, it is clear that it would be extremely worthwhile to calculate the predictions from this model for these experimentally measurable parameters and that should be compared to the present findings for a further insight on the dynamics of the polymer microstructure and the velocity-field.

## V. SUMMARY AND CONCLUSIONS

We have presented our results on the transient evolution of birefringence and orientation angle for a series of entangled polymer solutions subjected to the start-up flow at several Weissenberg numbers. An extensive study of these results along with the corresponding velocity-gradients for each Weissenberg number and for each sample, measured using a dynamic light scattering technique, is presented for the first-time for such extension-dominated time-dependent flows. As expected, there is a very significant flow-modification geared by the orientation and stretching of the polymer molecules. The measured flow kinematics show that the effect of the polymers on the flow in the immediate vicinity of the stagnation-point is to decrease its extensional strength (and the rate of strain) relative to the velocity-field for

a Newtonian fluid. This drastically changes the value of the steady-state  $Wi_R$  measured at the stagnation-point, which we have used to identify each transient experiment, from that imposed on the polymeric fluids. Similar results of polymer induced reduction of strain-rate at the stagnation-point of a two-roll mill was also obtained experimentally for dilute polymer solutions [17,21]. This observation was qualitatively interpreted [17,22], using a dumbbell model [26], from the fact that dilute solution of high molecular weight, linear, flexible polymers strongly strain-rate harden in extension-dominated flow [23]. In contrast, entangled polymeric fluids strain-rate soften over a considerable range of strain-rates in such flows and hence the experimentally observed similar behavior for these very different polymer concentrations seems to be quite remarkable. However, recent numerical studies by Remmelgas *et al.* [20], using a vector approximation of the DEMG model in a two-roll mill, have indeed predicted a decrease in the strain-rate at the stagnation-point for entangled polymeric fluids, in clear agreement with our experiments. They interpreted that this decrease results from the effect of a shear-thinning viscosity in the flow near the rollers which makes momentum transfer to the region between the rollers less efficient. This prediction is specific to the extension-dominated flows generated in the two-roll mill only.

We observed a very distinct coupling between the polymer conformational dynamics and the changes in the flow-field. The results for the time-dependent flows presented in this paper, the corresponding steady-state results in Part I [12], as well as some other studies from our laboratory [11] unequivocally emphasizes that the in the flow regime away from chain-stretching, these coupled dynamics are invariant to changes in polymer concentration and molecular weight, as long as the number of entanglements per chain is held fixed. On the inception of flows with similar Weissenberg numbers, an increase in the number of entanglements per chain was accompanied by increased overshoot and undershoot in the birefringence and by a slower response time, in addition to a decreased steady-state stretching of the polymer chains. There is an associated undershoot in the orientation angle data at high rates of deformation which is shifted to longer times compared to the first overshoot in the birefringence. The polymer induced flow behavior is very complicated. The variation of the magnitude of the flow-parameters over the total evolution time is very pronounced for the fluid with lowest  $Ne$ , in contrast to a weak effect found for the other two samples having similar value for  $Ne$ . There is a transition in the behavior of the polymer anisotropy as well as the coupled flow dynamics at some critical Weissenberg number specific to each system. The velocity-gradient component,  $\dot{\gamma}\lambda$ , and hence the flow-type parameter,  $\lambda$ , are more sensitive to the impact of evolution of the polymer microstructure, than the other velocity-gradient component,  $\dot{\gamma}$ .

The undershoot in the measured flow-parameters seem to be strongly correlated with the first overshoot in the birefringence and hence the first undershoot in the orientation angle data. The Newtonian-strain at the overshoot of birefringence for the polystyrene solutions shows qualitatively similar behavior to that found earlier [18,24] for the extension-dominated flows. The behavior for the measured strain, in contrast, differs from that because of the strong modification observed in the flow from the corresponding Newtonian-value. In similarity with that seen with dilute polymeric solutions [17,21], the flow with the entangled solutions too reduces its extensional character and becomes more viscometric or shear-like away from the stagnation-point although the underlying mechanism in these two cases was shown, in a recent theoretical work [20], to be very different from each other. The measured velocity-gradient shows different behaviors in the gap between the rollers depending on the orientation of the two-roll mill in the plane of the flow. At small Weissenberg numbers the flow-type parameters extracted from the dynamic light scattering results have values that are consistently higher than that would be expected for a Newtonian fluid. Our steady-state results [12] on the same polymeric fluids also support this finding. This is the first-time observation of such a behavior of the flow-type parameter for entangled polymer solutions in the range of small Weissenberg numbers for a strong, extension-dominated flow. The numerical simulations by Remmelgas *et al.* [20] have clearly shown, in direct similarity with our experimental results, that the flow-type parameter for entangled polymer solutions near the stagnation-point for this particular configuration of the two-roll mill does increase relative to the Newtonian-values, at small Weissenberg numbers. This point certainly deserves further careful experimental and theoretical studies, and ongoing experiments in our laboratory are intended to resolve this issue. Nevertheless, the results presented here provides an unique basis to crucially test the reptation based DEMG models with chain-stretching included. This can be done by using the experimentally measured time-dependent velocity-gradient as an input to the model and then comparing its prediction for the time-dependent birefringence and orientation angle to that obtained experimentally. Alternatively, for the range of parameters involved in this study, one can numerically simulate both the birefringence and velocity-field, using the computationally tractable vector approximation of the DEMG model [6], which could then be compared with the present experiments. In contrast to the first method, the second one simulates the predictions of both the effect of flow on polymers and the effect of polymers on flow. Work is underway in these directions.

## ACKNOWLEDGMENTS

We thank Johan Remmelgas and James P. Oberhauser for helpful discussions.

- 
- <sup>†</sup> Author for correspondence. Present address: Department of Physics and Astronomy, University of Pennsylvania, Philadelphia, PA 19104-6396, U.S.A. Electronic address: subrata@dept.physics.upenn.edu.
- <sup>\*</sup> Present address: Kimberly-Clark Co., Neenah, WI, U.S.A.
- [1] G. Astarita, *J. Non-Newtonian Fluid Mech.* **6**, 69 (1979); W. L. Olbricht, J. M. Rallison and L. G. Leal, *J. Non-Newtonian Fluid Mech.* **10**, 291 (1982); R. I. Tanner, *AIChE J.* **22**, 910 (1976).
  - [2] M. Doi and S. F. Edwards, *The Theory of Polymer Dynamics*, (Oxford U.P., New York, 1986).
  - [3] G. Marrucci and N. Grizzuti, *Gazzetta Chimica Italiana* **118**, 179 (1988); D. S. Pearson, E. Herbolzheimer, N. Grizzuti and G. Marrucci, *J. Polym. Sci. Polym. Phys. Ed.* **29**, 1589 (1991); D. W. Mead, E. A. Herbolzheimer and L. G. Leal, in *Theoretical and Applied Rheology*, Proceedings of the XIth International Congress on Rheology, edited by P. Moldenaers, and R. Keunings (Brussels, Belgium, 1992); D. W. Mead and L. G. Leal, *Rheol. Acta* **34**, 339 (1995); D. W. Mead, D. Yavich and L. G. Leal, *Rheol. Acta* **34**, 360 (1995).
  - [4] D. S. Pearson, A. D. Kiss, L. J. Fetters and M. Doi, *J. Rheol.* **33**, 517 (1989).
  - [5] R. Bird and J. DeAguiar, *J. Non-Newtonian Fluid Mech.* **13**, 149 (1983); R. Larson, *J. Rheol.* **28**, 545 (1984); G. Marrucci, *J. Non-Newtonian Fluid Mech.* **62**, 279 (1996).
  - [6] J. Remmelgas, G. Harrison, and L. G. Leal, *J. Non-Newtonian Fluid Mech.*, **80**, 115 (1999).
  - [7] B. E. Zebrowski and G. G. Fuller, *J. Polym. Sci.: Polym. Phys. Ed.* **23**, 575 (1985).
  - [8] J. P. Oberhauser, L. G. Leal and D. W. Mead, *J. Polym. Sci. Polym. Phys. Ed.* **36**, 265 (1998).
  - [9] G. G. Fuller, J. M. Rallison, R. L. Schmidt, and L. G. Leal, *J. Fluid Mech.* **100**, 555 (1980).
  - [10] J. J. Wang, D. Yavich and L. G. Leal, *Phys. Fluids* **6**, 3519 (1994).
  - [11] D. Yavich, Ph. D. Thesis, University of California, Santa Barbara, U.S.A., 1995 (unpublished); D. Yavich, D. W. Mead, J. P. Oberhauser and L. G. Leal, *J. Rheol.* **42**, 671 (1998).
  - [12] S. Sanyal, D. Yavich and L. G. Leal, manuscript in preparation (2000).
  - [13] J. P. Oberhauser, Ph. D. Thesis, University of California, Santa Barbara, U.S.A., in preparation.
  - [14] P. J. Flory, *Statistical Mechanics of Long Chain Molecules*, (Wiley Interscience, 1969).
  - [15] E. Geffroy and L. G. Leal, *J. Polym. Sci.: Polym. Phys. Ed.* **30**, 1329 (1992); E. Geffroy, Ph. D. Thesis, California Institute of Technology, U.S.A., 1991 (unpublished).



- [16] P. N. Dunlap and L. G. Leal, J. Non-Newtonian Fluid Mech. **23**, 5 (1987).
- [17] G. Harrison, Ph. D. Thesis, University of California, Santa Barbara, U.S.A., 1997 (unpublished); G. Harrison, J. Remmelgas and L. G. Leal, J. Rheol. **42**, 1039, (1998); *ibid* **43**, 197 (1999).
- [18] E. Geffroy and L. G. Leal, J. Non-Newtonian Fluid Mech. **35**, 361 (1990).
- [19] E. V. Menezes and W. W. Graessley, J. Polym. Sci. Polym. Phys. Ed. **20**, 1817 (1982).
- [20] J. Remmelgas, Ph. D. Thesis, University of California, Santa Barbara, U.S.A., 1998 (unpublished); J. Remmelgas and L. G. Leal, J. Non-Newtonian Fluid Mech. **90**, 187 (2000); *ibid*, 231 (2000).
- [21] R. -Y. Ng and L. G. Leal, J. Rheol. **37**, 443 (1993).
- [22] P. Singh and L. G. Leal, J. Rheol. **38**, 485 (1994); J. Non-Newtonian Fluid Mech. **67**, 137 (1996).
- [23] N. Orr and T. Sridhar, J. Non-Newtonian Fluid Mech. **67**, 77 (1996).
- [24] K. Koyama and O. Ishizuka, J. Polym. Sci. Polym. Phys. Ed. **27**, 297 (1989).
- [25] A. W. Chow and G. G. Fuller, J. Rheol. **28**, 23 (1984); G. G. Fuller, *Optical Rheometry of Complex fluids*, (Oxford University Press, Oxford, 1995).
- [26] M. D. Chilcott and J. M. Rallison, J. Polym. Sci. Polym. Phys. Ed. **29**, 381 (1988).

TABLE I. The characteristic parameters for the three polystyrene samples.

Sample	$M_w$ ( $\times 10^6$ )	$M_w/M_n$	$c$ ( $\frac{g}{cc}$ )	$\eta_0$ (P)	$N_e$	$\tau_R$ (s)	$n_t$
PS81	8.42	1.17	0.0396	7500	$\sim 13$	2.25	8420
PS82	8.42	1.17	0.0262	2700	$\sim 7$	3.01	8420
PS2	2.89	1.09	0.0867	19000	$\sim 13$	0.56	2890

TABLE II. The Weissenberg numbers [measured,  $Wi_R = \dot{\gamma}\lambda^{1/2}\tau_R$ , and the Newtonian,  $(Wi_R)_N = \dot{\gamma}_N\lambda_N^{1/2}\tau_R$ ] used for the three polystyrene samples and the percentage flow-modification.

PS82			PS81			PS2		
$(Wi_R)_N$	$Wi_R$	%	$(Wi_R)_N$	$Wi_R$	%	$(Wi_R)_N$	$Wi_R$	%
0.099	0.078	21.33	0.052	0.004	92.04	0.031	0.013	59.09
0.199	0.144	27.56	0.058	0.006	90.58	0.057	0.027	51.89
0.298	0.199	33.26	0.081	0.011	86.83	0.114	0.056	51.21
0.394	0.245	37.88	0.103	0.017	83.45	0.177	0.075	57.66
0.494	0.284	42.42	0.295	0.103	65.19	0.315	0.151	52.10
0.593	0.319	46.20	0.443	0.181	59.15	0.400	0.215	46.32
0.792	0.384	51.49	0.592	0.266	55.04	0.429	0.236	45.00
0.990	0.455	54.05	0.889	0.470	47.13	0.468	0.263	43.82
1.385	0.636	54.07	1.183	0.699	40.95			
1.782	0.843	52.70						